Environ. Sci. Technol. **2005**, *39,* 4938−4952

Deconvolution and Quantification of Hydrocarbon-like and Oxygenated Organic Aerosols Based on Aerosol Mass Spectrometry

QI ZHANG,[†] M. RAMI ALFARRA,[§,⊥] DOUGLAS R. WORSNOP,[∥] JAMES D. ALLAN,[§] HUGH COE,[§] MANJULA R. CANAGARATNA,[∥] AND JOSE L. JIMENEZ*[,†,‡]

Cooperative Institute for Research in Environmental Sciences (CIRES) and Department of Chemistry and Biochemistry, 216 UCB, University of Colorado-Boulder, Boulder, Colorado 80309-0216, School of Earth, Atmospheric and Environmental Science, Main Building, Sackville Street, University of Manchester, Manchester M60 1QD, U.K., and Aerodyne Research Inc., Billerica, Massachusetts 01821-3976

A new technique has been developed to deconvolve and quantify the mass concentrations of hydrocarbon-like and oxygenated organic aerosols (HOA and OOA) using highly time-resolved organic mass spectra obtained with an Aerodyne Aerosol Mass Spectrometer (AMS). This technique involves a series of multivariate linear regressions that use mass-to-charge ratios (*m*/*z*'s) 57 (mostly $C_4H_9^+$) and 44 (mostly CO_2^+)—the identified AMS mass spectral tracers for HOA and OOA, respectively—as the initial principal components. Two algorithms have been developed: algorithm 1 is based solely on *m*/*z* 44 and *m*/*z* 57, and algorithm 2 is an iterative procedure expanded from algorithm 1. This technique was applied to the AMS organic aerosol data acquired at the EPA Pittsburgh Supersite during September 2002. The reconstructed organic concentrations (= HOA + OOA) agree well with the measured values (r^2 = 0.997, slope = 0.998), and the reconstructed organic data matrix (size = 3199 time steps × 300 *m*/*z*'s) explains 99% of the variance in the measured time series. In addition, the extracted mass spectrum of HOA shows high similarity to those of diesel exhaust, lubricating oil, and freshly emitted traffic aerosols observed in urban areas, while the spectrum of OOA closely resembles those of aged organic aerosols sampled in rural areas and also shows similarity with the spectrum of fulvic acid—a humic-like substance that is ubiquitous in the environment and has previously been used as an analogue to represent polyacid components found in highly processed and oxidized atmospheric organic aerosols. There is evidence for the presence of a third component, although its contribution to the total organic signal appears to be small in this study. The most important result is that *m*/*z* 44 and *m*/*z* 57 are reliable AMS mass spectral "markers" that provide the "first guess" for algorithm 2 which allows the quantitative description of the organic aerosol concentration and mass spectra over a period of 16 days in a major urban area and allows the extraction of mass spectra of OOA and HOA that can be interpreted chemically. These findings indicate the potential of performing organic source apportionment on the basis of total particle mass, rather than on the basis of organic tracer compounds that contribute a small fraction of this mass.

Introduction

Organic material comprises a significant, yet poorly characterized, fraction of the fine particles in the atmosphere (*1*−*4*). The number and complexity of particulate organic compounds make it a significant challenge to fully characterize their molecular identities (*1, 2*). Analysis of a large number of molecules, for example, typically accounts for only a minor fraction of the organic carbon in aerosols (*5*−*7*). As a result, there is only a limited understanding of the chemistry, sources, and processing of organic aerosols, and assessments of their impacts on climate, visibility, and human health remain notably uncertain (*1, 6, 8, 9*).

Organic aerosols originate from many different natural and anthropogenic sources and processes. Primary organic aerosols (POA) are those emitted directly into the atmosphere in particle form, e.g., from fossil fuel and biomass combustion, while secondary organic aerosols (SOA) are formed from gaseous precursors through gas-phase (*1, 2, 6*), particle-phase (*10*), or aqueous-phase reactions (*11, 12*). Due to their different origins and formation mechanisms, POA and SOA usually demonstrate very different chemical and microphysical properties (*13*−*18*). Therefore, to design effective fine particle control strategies and to better evaluate the roles of organic aerosols in regional and global climate we must understand the concentrations, properties, and sources of these two organic aerosol types (*6*).

Three general techniques are available to estimate the relative contributions of POA and SOA to ambient particle mass. One is "source-oriented" chemical transport models (CTMs) that simulate atmospheric transport and chemical reactions (*6, 19*−*21*). Another is "source-receptor" methods that interpret ambient measurements with a mathematical model that uses distinctive tracers and previous knowledge of the tracer concentrations in all known sources (*6, 22, 23*). Commonly applied organic source-receptor methods include the organic molecular marker chemical mass balance (CMB) method (*22*−*24*) and the organic carbon (OC) to elemental carbon (EC) ratio method (*25*−*29*). The third is receptor-only methods, which are conceptually similar to principal component analysis (*30*) and use statistical multivariate techniques to extract source information from the time series of multiple simultaneous measurements. Commonly used receptor methods for air pollution studies include Positive Matrix Factorization (PMF) (*31*) and UNMIX (*32*).

Unlike "source-oriented" CTMs, source-receptor and receptor methods do not require detailed information on meteorology or emission inventories but instead perform source apportionment using ambient measurements as inputs (*6*). So far, receptor methods have been relatively successful with POA applications but show limited capability to distinguish the sources of SOA components unless

* Corresponding author phone: (303)492-3557; fax: (303)492-1149; e-mail: jose.jimenez@colorado.edu.

[†] Cooperative Institute for Research in Environmental Sciences (CIRES), University of Colorado-Boulder.

[‡] Department of Chemistry and Biochemistry, University of Colorado-Boulder.

[§] University of Manchester.

[∥] Aerodyne Research Inc.

[⊥] Present address: Paul Scherrer Institute, 5232 Villigen PSI, Switzerland.

10.1021/es048568l CCC: $30.25
Published on Web 05/27/2005

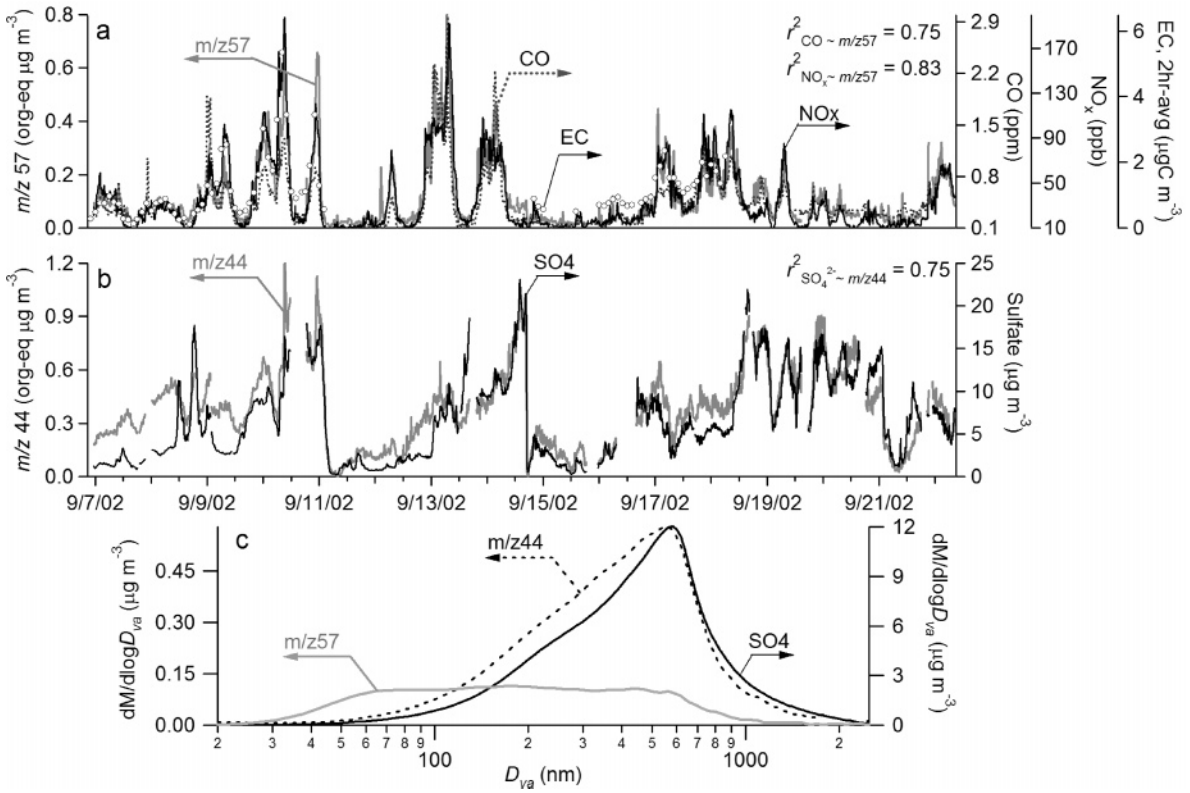

FIGURE 1. Time trends of (a) *m/z* 57 and typical combustion emission tracers (CO, NO_x, EC) and (b) *m/z* 44 and PM_1 SO_4^{2-} (both from the AMS) and (c) the average size distributions of *m/z* 44, *m/z* 57 and SO_4^{2-} during the AMS deployment at the Pittsburgh Supersite.

combined with CTMs (*6*). For these reasons, in both CMB (*20, 23, 33*) and OC/EC methods (*25−29*), the SOA concentration is usually inferred as the difference between observed organic aerosol mass concentrations and estimated POA. A major drawback of this approach is that the accuracy of predicted SOA concentration is poor when POA values are uncertain. Recently, tracers for SOA, such as aromatic diacids, have been proposed (*24, 34, 35*), but the ability to use them to quantitatively estimate SOA concentrations has not yet been demonstrated.

Methods that are capable of estimating the contributions of SOA and POA independently are needed. In this study we have developed a new technique that can determine the mass concentrations of hydrocarbon-like and oxygenated organic aerosols based on the mass spectra of ambient particles acquired by an Aerodyne Aerosol Mass Spectrometer (AMS). The AMS is a real-time aerosol instrument that samples, sizes, and analyzes nonrefractory submicron particles (NR-PM_1) with high sensitivity and time and size resolution (*18, 36−44*). It is currently the only real-time instrument with the potential to provide quantitative and size-resolved organic aerosol data with a time resolution of minutes.

The quantitative capabilities of the AMS arise from the combination of a quantitative aerosol sampling using an aerodynamic lens (*38, 45−47*) and the separation of particle vaporization and vapor ionization processes (*36, 38*). The AMS employs thermal vaporization (usually at 600 °C) on a porous tungsten conical surface operated under high vacuum, followed by 70 eV electron impact (EI) ionization. Matrix effects due to charge-transfer reactions occurring during collisions between vapor molecules and ions (*48*) are eliminated due to the high vacuum conditions under which ionization takes place. If the species are vaporized intact, their AMS spectra are generally similar to the standard EI spectra such as in the NIST database (*49*). However, thermally labile species may undergo decomposition upon vaporization or greater fragmentation due to the higher internal energy acquired during vaporization. For these reasons the spectra observed in the AMS may show greater fragmentation than standard EI spectra (*50*) (and unpublished data from Philip Silva, Utah State University).

The ion signal recorded by the AMS at each mass-to-charge ratio (m/z) is a linear combination of those from individual vaporized species in the analyte (*36, 40*). As such, an AMS mass spectrum, which is a distribution of ion signals with unit m/z resolution, typically between 1 and 300 m/z, is essentially the linear superposition of the distinctive mass spectra of individual species that produce signals. Currently, a standard AMS data analysis method is available to systematically deconvolve the ensemble AMS mass spectra into partial mass spectra for distinct species or groups of species, such as NO_3^-, NH_4^+, SO_4^{2-}, Cl^-, and organics (*40*). The inputs to this mathematical method are isotopic ratios of elements and laboratory-measured AMS fragmentation patterns, e.g., for major gaseous species (N_2, O_2, Ar, H_2O, and CO_2) and aerosol inorganic species. The fragmentation patterns approach, however, only allows the extraction of the mass spectra for total organics and provides no information about subcomponents of organic aerosols.

The linearity inherent in the AMS organic mass spectra, together with the high time resolution of their measurements, provide the foundation for a multivariate "receptor-only" analysis approach to unravel the main types of organic aerosols present in the atmosphere. We present here a technique of this nature. Our technique allows quantitative deconvolution of AMS organic aerosol data from urban areas into two major components—hydrocarbon-like and oxygenated—and provides information on their characteristics (mass spectra, time evolution, and size distributions). This paper focuses on the development and validation of the method by applying the technique to the Pittsburgh Supersite data set. The major findings regarding these two types of organic aerosols in Pittsburgh will be presented separately (Zhang et al., in preparation for *Atmos. Chem. Phys.*). Future papers

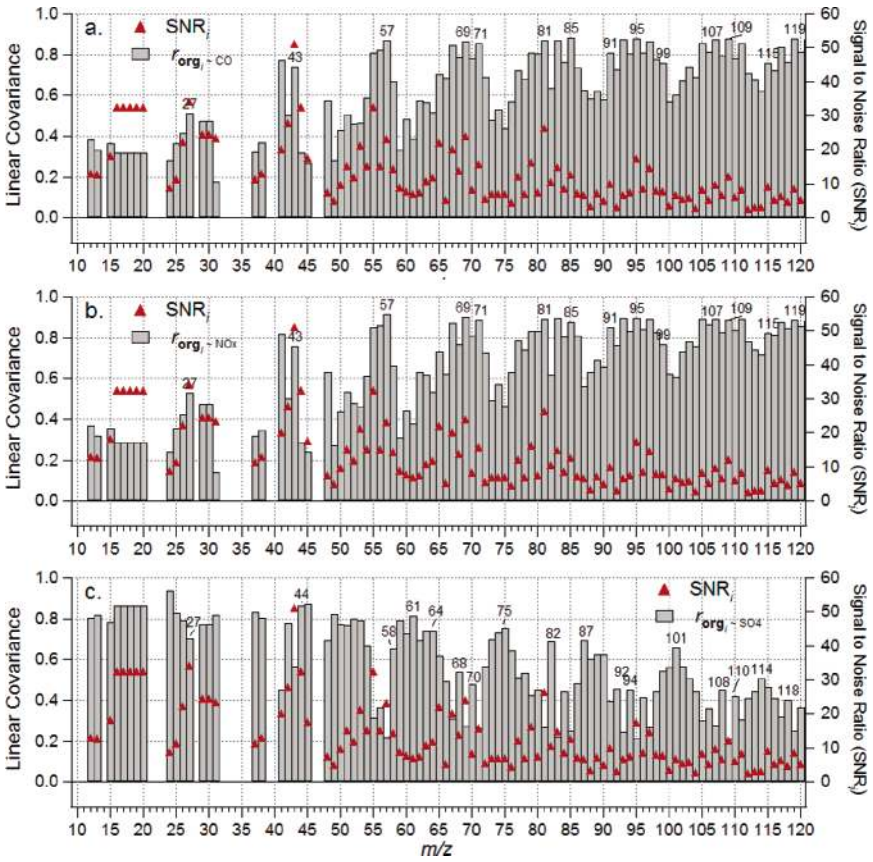

FIGURE 2. Covariance plots of (a) CO to organic *m/z*'s (org$_i$); (b) NO_x to org$_i$; and (c) SO_4^{2-} to org$_i$. The red triangles are the average signal-to-noise ratios for org$_i$ (SNR$_i$). See section entitled "Notation" for notation.

will extend the application of the technique to other urban, rural, and remote locations in which AMS data has been acquired.

Methods

Data Preparation. The AMS data set used in this study was acquired during September 7th−22nd, 2002 from the main site of the Pittsburgh Air Quality Study (PAQS) and EPA Supersite. Detailed information on sampling, AMS operation, and analysis for this data set is presented in two previous papers (*18, 51*). The theory, underlying assumptions, and technical details of the data analysis procedures have been described previously (*36, 39−41*). The standard AMS data analysis software and the computational codes for data reduction and numerical analysis developed for this study were written in Igor Pro 5 (Wavemetrics, Inc., Lake Oswego, Oregon).

A total number of ~3200 aerosol organic mass spectra (averaging time = 10 min initially and = 5 min after September 12) were acquired in Pittsburgh. Each of them is expressed as a 300-element vector, corresponding to the number of mass-to-charge ratio channels scanned (i.e., m/z 1−300). Note that only 270 out of the 300 m/z's contain organic signals. The other 30 (m/z's 1−11, 14, 21−23, 28, 32−36, 39−40, 46−47, 149, 182−184, and 186) were omitted due to either the lack of plausible organic fragments (e.g. m/z 3), the overwhelming contributions from inorganic (e.g., m/z 39) or gaseous species (e.g., m/z 32), or the high background level in the instrument (e.g., m/z 149) (*40*). In addition, values of m/z's 16, 17, 18, and 20 in the organic mass spectral matrix were not calculated from the raw signals at these channels due to the excessive interfering signals from water but rather set to be proportional to the organic signals at m/z 44, based on laboratory experiments (unpublished data from Philip Silva, Utah State University). The intensity of each peak in a mass spectrum is expressed in organic-equivalent mass concentration (org-eq, in μg m^{-3}) calculated from the raw signals in ions per second (Hz) (*36, 39−41*). The org-eq concentration is defined here as the mass concentration of organics that would produce the same signal intensity (summed over all 270 m/z's) as that observed at one individual m/z. It differs from the nitrate-equivalent mass concentration (NO_3^--eq) in that the relative ionization efficiency factor (RIE) for organics (*36, 41*) is applied to NO_3^--eq to yield org-eq concentrations. The sum of org-eq concentrations of all m/z's in an organic mass spectrum yields the total organic mass concentration. We observed good agreement between the AMS organic mass concentrations and 2 h-averaged organic carbon data from a collocated thermal optical transmittance carbon analyzer (Sunset Labs; $r^2 = 0.88$; Slope (S) = 1.69; $N = 82$) and 24 h-averaged OC data from filter samples post-analyzed with the thermal-optical technique ($r^2 = 0.64$; $S = 1.45$; $N = 14$) (*18*). Similar agreement has been observed in studies in Houston and Tokyo (*52, 53*).

(a) Pretreatment for Organic Mass Spectral Data. Minor filtering was performed on the raw organic mass spectral data to reduce high-frequency noise. First, 6 mass spectra (~1 h worth of data) sampled during 18:50−19:40 on September 8 were excluded from this study since they were strongly influenced by a narrow organic plume of high concentration (peak ≈ 50 μg m^{-3} vs 4 μg m^{-3} for the average organic mass concentration of the entire study) (*18*). The average mass spectrum of the component represented by this plume shows more similarity to HOA than OOA (Supporting Information, Figure S1).

We also reduced sporadic spikes in isolated m/z's (i.e., sudden surges in signal) for this study. A spike is

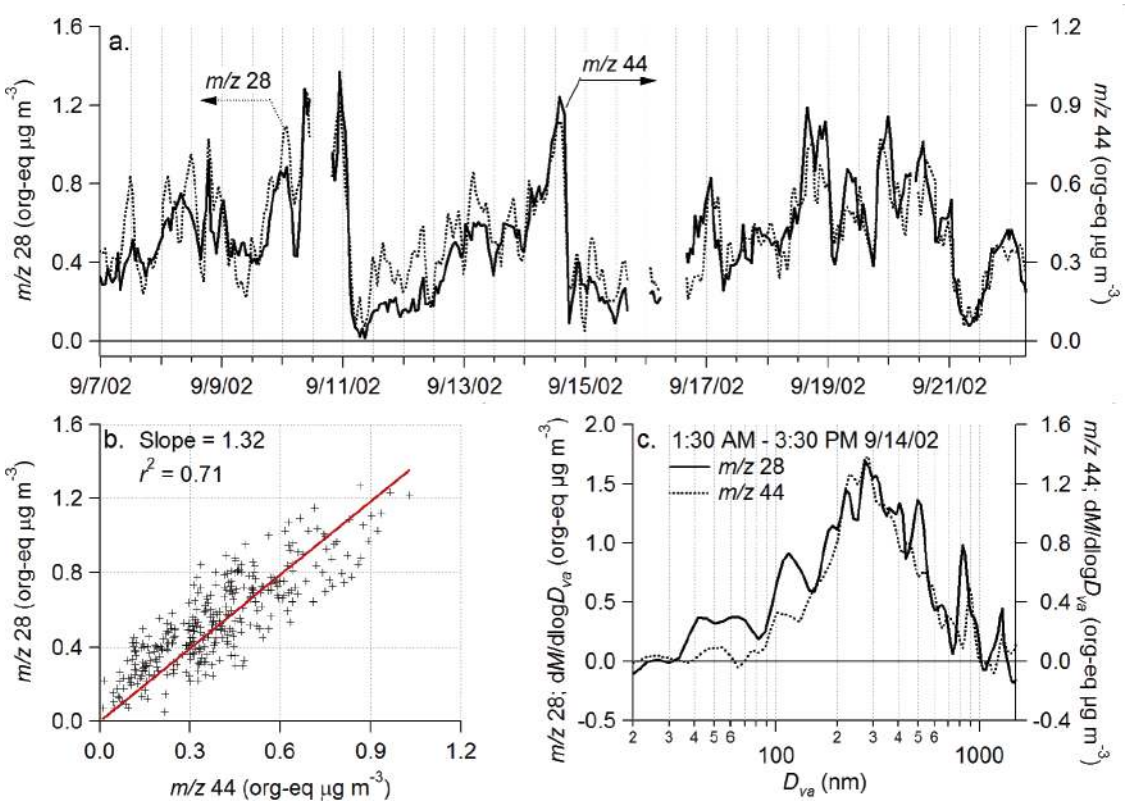

FIGURE 3. (a) Hourly averaged signal intensities (org-eq μg m^{-3}) of *m/z* 44 and *m/z* 28 derived from the AMS P-TOF data. (b) Scatter plot comparing the hourly averaged signal intensities of *m/z* 28 and *m/z* 44, the red line is the least-squares linear fit with the intercept forced to zero. (c) Average size distribution of *m/z*'s 28 and 44 during a high signal-to-noise ratio period. A similar size distribution comparison, albeit typically noisier, is observed during other time periods.

identified when a signal is at least 2 times larger than the larger one of its two immediate neighbors in the time series. Two reasons are likely responsible for the observed infrequent spikes in some organic m/z's. One is poor sampling statistics of the AMS for particles with high mass but low number concentration (~1 cm^{-3}) in the air. These particles produce a spike in only one or a few m/z's during an AMS averaging time step (~5 min) because the AMS scans only one m/z at a time (see Table 2 of Bahreini et al. (*54*) for details on AMS sampling statistics). Since the average mass spectrum and time variation of the spikes look similar to the component mass spectrum of hydrocarbon-like organic aerosols (see section entitled "Linear Covariance Analysis" and Supporting Information Figure S2), these particles appear to mainly associate with combustion sources (e.g., traffic), which is supported by results from AMS "chase-mode" sampling of individual vehicles that show a larger mode in vehicle exhaust (*55*). Another possible (less likely) reason for the occurrence of the spikes is the bounce of larger particles in the AMS detection region so that some could land on the electron emission filament, evaporate, and be ionized with higher efficiency. This phenomenon may explain some infrequent larger signals observed during the AMS size calibration with large (>800 nm) polystyrene latex spheres (PSLs) but has not yet been conclusively observed in ambient sampling. Overall, we found that these spikes occur rather infrequently (<1% of the total data points) and account for only ~1% of the total organic signal. For these reasons they are unimportant for general applications, when only the mass concentrations of total organics is concerned. However, they represent a significant source of high-frequency variability in the time series of some individual m/z's and need to be dealt with for improved statistical analysis. To do so, we replaced these spikes with linear interpolation of the two adjacent values. Finally we applied a 3-point boxcar smoothing to the time series of each m/z to further reduce high-frequency noise in the data.

These three filtering operations were validated by performing exactly the same analysis on the treated and untreated data sets (see the Supporting Information Figures S3−S9 for analysis results on the untreated data set). The first step, i.e., removing the 1-h organic spike on September 8, produces a small but noticeable change in the results of this procedure, since the very high concentrations during this spike resulted in large χ^2 values that are weighed heavily in the analysis. Removing this spike allows us to better capture the characteristics of the HOA and OOA components during most of the study. Significant (~5−10%) improvements on χ^2's and r^2's have been observed for the data set treated for sporadic spikes compared to the untreated. The time trends and mass spectra of HOA and OOA derived from the filtered and unfiltered data are in good agreement (see Figure S10 in the Supporting Information), indicating that these pretreatments have effectively reduced artifacts due to limited sampling statistics yet preserved most of the information content of the data.

(b) Quantification of Particle Signal at m/z 28. A key feature of the AMS is that it uses a thermal vaporizer, on which the nonrefractory components of particles evaporate under high vacuum (~10^{-8} Torr) before electron impact (EI) ionization. In field studies, the vaporizer is often operated at ~600 °C, a temperature required for the fast evaporation of ammonium sulfate that is necessary to measure its size distribution. At this temperature, thermally labile oxygenated organic compounds may undergo pyrolysis, forming CO, CO_2, H_2O, and other vaporized species that diffuse into the EI ionization region (*40, 50*).

Both CO and CO_2 may produce signals at m/z 28 (CO^+) (*49*). However, gas-phase N_2 also produces m/z 28 signal (N_2^+) and generally at an intensity more than 2 orders of magnitude larger than particle signals during typical ambient studies (*40*). Note that since the AMS inlet reduces gaseous species by a factor of 10^7 (relative to the particles) gas-phase CO is not detectable and gas-phase CO_2 represents a very small contribution to m/z 28 at their typical ambient concentrations (*40*). Since the m/z 28 signals are almost pure N_2^+ they are typically used as the "internal standard" in AMS quantification to correct for variations in sampling flow rate and detector sensitivity. For these reasons, the entire m/z 28 signal is conventionally assigned to gaseous N_2^+ signals and is not reported in the AMS spectra of particles.

The particulate CO^+ signals (produced from oxygenated species) can be separated from the gaseous N_2^+ signals based on their very different flight velocities in the AMS (*18*). We therefore extracted the size distribution and mass concentration of particulate m/z 28 signals from the AMS particle time-of-flight (P-TOF) data using the technique developed by Zhang et al. (*18*). Because of the substantial tailing of the gaseous N_2^+ signals into the particle region, the subtracted particulate m/z 28 signals are much noisier than the other organic signals.

(c) Error Estimation and Signal-to-Noise Ratio Calculations. Errors associated with the mass spectral signals were estimated based on electronic noise and ion counting statistics (*36, 39*). As the mass spectral signals, the unit of errors is expressed as org-eq (μg m^{-3}). The signal-to-noise ratio (SNR) of a given signal is defined as the ratio of its intensity to the corresponding estimated error. The SNR of the total organic mass concentration is calculated based on the detection limit of the organic measurement (D.L. = 0.15 μg m^{-3}), which was estimated from several periods in which particle-free ambient air was sampled into the AMS during the study (*18*).

Mathematical Deconvolution Techniques. *(a) Notation.* Throughout this text, the following mathematical notation is used (*30*). Matrices are symbolized with bold uppercase letters and vectors with bold lowercase letters. Row vectors are marked with a prime (′) in order to be distinguished from column vectors. Scalar quantities and elements of vectors or matrices are represented by lowercase italic letters. The hat, "∧", above a quantity (vector, matrix, or scalar) indicates that it is calculated or estimated, rather than measured.

The entire organic mass spectral data set is expressed as a matrix of N_t rows by N_i columns (designated as **ORG**; in org-eq μg m^{-3}), in which each row corresponds to a time step (t) and each column corresponds to a mass-to-charge ratio (i). In other words, each row in **ORG** is a mass spectrum at a given point in time, and each column the time series of the org-eq mass concentration of a specific m/z. Specific quantities related to the **ORG** matrix are denoted as follows:

$ORG_{t,i}$ is the tth row and the ith column element in **ORG**, containing the org-eq concentration (μg m^{-3}) of the fragment $m/z = i$ measured at time step t.

$\mathbf{org}_t'$ is the tth row vector (also called "m/z vector") in **ORG**, i.e., the mass spectrum of organic aerosols measured at time t. For example, $\mathbf{org}'_{1000}$ is the organic mass spectrum recorded in time step 1000 (i.e., 10:00 A.M. − 10:05 A.M. on 9/12/2002 for the Pittsburgh study). The factor space of $\mathbf{org}_t'$, i.e., the number of m/z channels scanned, is N_i dimensional (N_i = 270 for the Pittsburgh data set).

$\mathbf{org}_i$ is the ith column vector (also called "time series vector") in **ORG**, i.e., the time series of the fragment $m/z = i$ of the entire study. For example $\mathbf{org}_{44}$ and $\mathbf{org}_{57}$ denote the time series of m/z 44 and m/z 57, respectively. The factor space of org_i, i.e., the number of mass spectra (time steps) measured, is N_t dimensional (N_t = 3199 for the Pittsburgh data set).

om is the time series of total organic mass concentrations; it equals the sum of org_i, i.e.

$$\mathbf{om} = \sum_{i=1}^{N_i} \mathbf{org}_i \tag{1}$$

$\mathbf{ms}'$ is the average mass spectrum of organics of the entire period

$$\mathbf{ms}' = \frac{1}{N_t}\sum_{t=1}^{N_t} (\mathbf{org}_t') \tag{2}$$

$\hat{\mathbf{ORG}}$ is an estimation of **ORG**, e.g., calculated using a linear model. Similarly, $\hat{\mathbf{org}}_i$ and $\hat{\mathbf{org}}_t'$ are the estimates of $\mathbf{org}_i$ and $\mathbf{org}_t'$, respectively, from the linear model.

(b) Mathematical Formulation. Given the linearity inherent in the organic mass spectra from an AMS, multivariate factor analysis can be used to investigate the major components that contribute to the total signals. The physical basis of this type of analysis is mass conservation (*30*). The mass balance equation for **ORG** (the N_t by N_i mass spectral matrix) is expressed as

$$\mathbf{ORG} = \mathbf{C} \cdot \mathbf{MS} + \mathbf{E} \tag{3}$$

where **C** is an N_t by N_c matrix containing the time series of the mass concentration of each of N_c components, **MS** is an N_c by N_i matrix containing the component mass spectra, and **E** is the error (residual) matrix. Therefore, by solving for **C** and **MS**, one may be able to extract the mass concentrations and mass spectra of major organic aerosol "factors", each of which may be due to an individual source or to several sources that covary in time or that have very similar chemical compositions.

(c) Custom Solution Procedure. Several multivariate techniques such as factor analysis (FA)/principal component analysis (PCA) (*30, 56*), positive matrix factorization (PMF) (*31*), and/or UNMIX (*32*) can be used to estimate **C** and **MS**. PCA has been used previously in the analysis of an AMS lab study (*57*). However, to yield physically meaningful results, factor analysis techniques usually involve a rather arbitrary procedure—rotation of the principal factor axis (e.g. "varimax" rotation)—that potentially makes the results questionable and has been the subject of much debate (*30, 58, 59*). In this study, instead of running a standard PCA-type technique, we take advantage of our a priori understanding of the AMS organic data and use two mass spectral marker peaks (m/z's 44 and 57) as the first-guess principal components. Iterative multiple multivariate linear regressions along the row and column dimensions of the organic matrix are then used to extract the component mass spectra and refine the component time series. Note that the major assumptions for factor analysis modeling listed in section 24.1.2 (p 1262) of Seinfeld and Pandis (*58*) also hold for this study.

Two simple multivariate linear regression algorithms have been developed. Algorithm 1 performs least-squares fits to the time series of organics mass concentration (**om**) and to the time series of individual m/z's ($\mathbf{org}_i$), as a linear combination of the measured time series of m/z's 44 and 57 (i.e., $\mathbf{org}_{44}$ and $\mathbf{org}_{57}$, respectively)

$$\mathbf{om} = a \cdot \mathbf{org}_{44} + b \cdot \mathbf{org}_{57} + \epsilon \tag{4}$$

$$\mathbf{org}_i = a_i \cdot \mathbf{org}_{44} + b_i \cdot \mathbf{org}_{57} + \epsilon_i \tag{5}$$

where, a, b, a_i, and b_i are the fitted parameters, ϵ and ϵ_i are the residual vectors (of dimension N_t), and the subscript i represents any m/z from 1 to N_m. We observe that $a \approx \Sigma_{i=1}^{N_i} a_i$ and $b \approx \Sigma_{i=1}^{N_i} b_i$ for this study.

Row vectors $\mathbf{a}'$ and $\mathbf{b}'$ are obtained by compiling a_i and b_i

$$\mathbf{a}' = \lfloor a_1 \ \cdots \ a_i \ \cdots \ a_{Ni} \rfloor \quad (6)$$

$$\mathbf{b}' = \lfloor b_1 \ \cdots \ b_i \ \cdots \ b_{Ni} \rfloor \quad (7)$$

where N_i is the number of m/z's in the matrix. We derive the component mass spectra of OOA and HOA by normalizing $\mathbf{a}'$ and $\mathbf{b}'$ to the sum of their respective elements (i.e., $\Sigma_{i=1}^{N_i} a_i$ and $\Sigma_{i=1}^{N_i} b_i$, respectively). Note that the numeric intensity of an m/z peak in these mass spectra is its percentage of the summed intensity of all peaks (i.e., % of $\Sigma m/z$). This is different from scaling the largest ("base") peak to 100 (i.e., relative intensity), as is commonly done in mass spectrometry (*49, 60*).

In algorithm 2, $\mathbf{a}'$ and $\mathbf{b}'$ are subsequently used to reconstruct each measured mass spectrum and thus produce two column vectors, $\mathbf{c}$ and $\mathbf{d}$

$$\mathbf{org}_t' = c_t \times \mathbf{a}' + d_t \times \mathbf{b}' + \epsilon_t' \quad (8)$$

$$\mathbf{c} = \begin{bmatrix} c_1 \\ \vdots \\ c_t \\ \vdots \\ c_{N_t} \end{bmatrix} \text{ and } \mathbf{d} = \begin{bmatrix} d_1 \\ \vdots \\ d_t \\ \vdots \\ d_{N_t} \end{bmatrix} \quad (9)$$

where c_t and d_t are the fitted parameters, the subscript t signifies a time step, and ϵ_t' is the residual vector. In principle, $\mathbf{c}$ and $\mathbf{d}$ are the improved time series of OOA and HOA, respectively, and therefore supersede $\mathbf{org}_{44}$ and $\mathbf{org}_{57}$ to derive improved OOA and HOA component mass spectra

$$\mathbf{org}_i = a_i \cdot \mathbf{c} + b_i \cdot \mathbf{d} + \epsilon_i \quad (10)$$

Equations 8 and 10 are the building blocks of algorithm 2, which iteratively generates a sequence of $\mathbf{a}'$, $\mathbf{b}'$, $\mathbf{c}$, and $\mathbf{d}$ vectors by performing least-squares linear regressions on **ORG** alternatively along the row dimension and the column dimension:

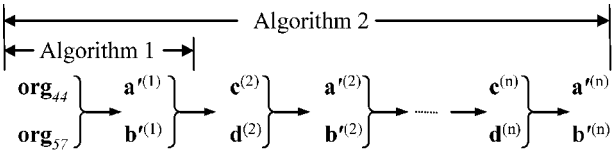

(11)

where n indicates the number of iterations.

The performance of both algorithms is evaluated by comparing ϵ, ϵ_i, and ϵ_t' to the corresponding analytical uncertainties, which are defined as the detection limits or 3 times the estimated errors (see section entitled "Error Estimation and Signal to-Noise Ratio Calculations").

(d) Calculations of Reconstructed Matrix and Residuals. The organic matrix reconstructed for a given iteration (n), $\mathbf{O\hat{R}G^{(n)}}$, is calculated from the corresponding row vectors, $\mathbf{c^{(n)}}$ and $\mathbf{d^{(n)}}$, and column vectors, $\mathbf{a'^{(n)}}$ and $\mathbf{b'^{(n)}}$:

$$\mathbf{O\hat{R}G^{(n)}} = \mathbf{c^{(n)}} \cdot \mathbf{a'^{(n)}} + \mathbf{d^{(n)}} \cdot \mathbf{b'^{(n)}} \quad (12)$$

The tth row and the ith column element of $\mathbf{O\hat{R}G^{(n)}}$ is calculated as

$$O\hat{R}G_{t,i}^{(n)} = c_t^{(n)} \cdot a_i^{(n)} + d_t^{(n)} \cdot b_i^{(n)} \quad (13)$$

where, respectively, $c_t^{(n)}$ and $d_t^{(n)}$ are the tth elements in $\mathbf{c^{(n)}}$ and $\mathbf{d^{(n)}}$, and $a_i^{(n)}$ and $b_i^{(n)}$ are the ith elements in $\mathbf{a'^{(n)}}$ and $\mathbf{b'^{(n)}}$. $\mathbf{org}_{44}$ and $\mathbf{org}_{57}$ are equivalent to $\mathbf{c^{(1)}}$ and $\mathbf{d^{(1)}}$. The residual of a fit is calculated as the difference between measured and reconstructed values. To avoid possible under-representation of the residual of organic mass concentration, which is caused by the cancellation of positive and negative values, we also calculated the absolute residual of the reconstructed vs measured organic mass concentration as the sum of the absolute values of the errors at each m/z ($Organics_t^{resid}$):

$$Organics_t^{resid} = \sum_{i=1}^{300} |(O\hat{R}G_{t,i}^{(n)} - ORG_{t,i})| \quad (14)$$

(e) Statistical Evaluation. Pearson's r is used extensively in this study to evaluate the strength of an observed correlation. However, since r is ignorant of the individual distributions of the two variables, by itself is a rather poor statistic for deciding the statistical significance of a correlation (*61*). We therefore calculated p-values, the probability of a null hypothesis, to evaluate the statistical significance of each observed r (*61*). A small p-value indicates that the degree of correlation signified by r is statistically significant (*61*). For this study all calculated p-values are substantially less than 10^{-3} ($\ll$0.1%), indicating that every r value reported is statistically significant. The p-values are thus not reported to avoid clutter.

Results and Discussion

Identification of Mass Spectral Tracers for Hydrocarbon-like and Oxygenated Organics. *(a) Summary of Previous Evidence.* According to laboratory and field studies, m/z 44 (most likely CO_2^+) is frequently a major peak in the AMS mass spectra of oxygenated organic species, (*41, 50*) and m/z 57 (mostly likely $C_4H_9^+$) is a major peak in the spectra of hydrocarbons and is typically associated with combustion exhaust (*41, 44, 51, 55, 62*). m/z 57 in AMS aerosol spectra often increases during the rush hours in urban areas, while m/z 44 usually dominates the spectra of heavily oxidized organic particles from rural areas and increases in the afternoon when photochemistry is more intense (*18, 41, 51*). In addition, the size distribution of m/z 44 in ambient particles is generally dominated by the accumulation mode and closely resembles that of sulfate (*18, 41, 51, 62, 63*), whereas that of m/z 57 in urban areas almost always displays a prominent ultrafine mode that is clearly associated with vehicular emissions (*18, 41, 44, 51, 55, 62, 63*). In view of these facts m/z 57 appears to be an AMS mass spectral fingerprint for particles from primary combustion sources and m/z 44 for oxygenated organic particles that are potentially associated with secondary organic aerosols or oxygen-containing primary organic aerosols.

(b) Additional Evidence for Tracer m/z's from Pittsburgh Supersite Data. To further justify the use of these two tracer m/z's, we present in Figure 1a the time series of m/z 57 and CO, NO_x, and elemental carbon (EC)—all well-known markers of combustion exhaust (*64*). Figure 1b shows the time series of m/z 44 and sulfate—a particulate species that is mainly formed through gas-phase and aqueous-phase oxidation of SO_2. Good correlations are observed between m/z 57 and CO ($r^2 = 0.75$), NO_x ($r^2 = 0.83$), and EC ($r^2 = 0.78$), supporting the use of m/z 57 as a first-order tracer for combustion related hydrocarbon-like organic particles. Good correlation is also observed between m/z 44 and SO_4^{2-} ($r^2 = 0.75$) which suggests that similar sources and/or processes over regional scales produce SO_4^{2-} and the parent organic species of m/z 44. These observations are consistent with the size distributions (Figure 1c)—those of m/z 44 and sulfate are both dominated by the accumulation mode, while that of m/z 57 demonstrates a prominent ultrafine mode that is commonly associated with combustion aerosols.

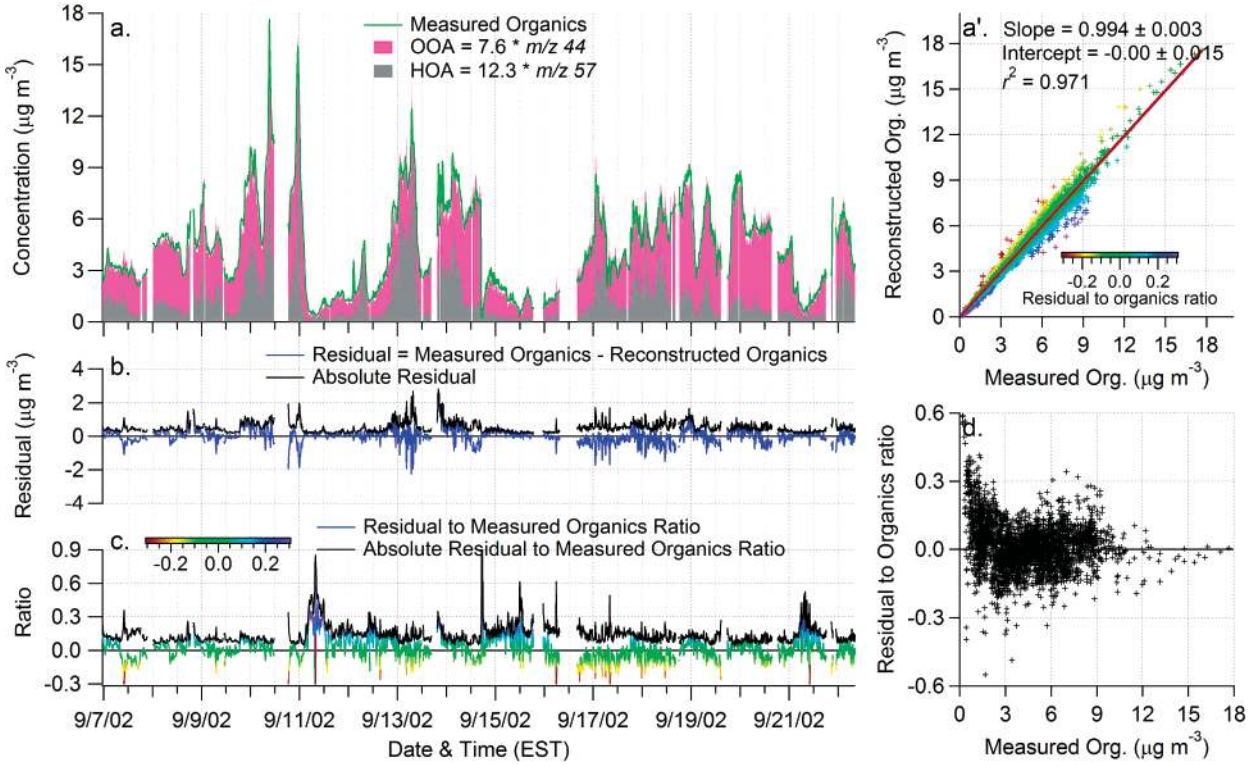

FIGURE 4. Results of algorithm 1: (a) time series of the measured organic mass concentration and HOA and OOA estimates (OOA is stacked on top of HOA); (a′) the scatter plot and linear fit (red line) between measured and reconstructed (= HOA + OOA) organic values; (b) variations of the residual of the fit (= measured − HOA − OOA) and the absolute residual (see section entitled "Calculations of Reconstructed Matrix and Residuals" for calculation) as a function of time; (c) time series of the ratio of the residual to the measured organic concentration; and (d) the scatter plot between the residuals and measured organic concentration. (a′) and (c) are colored by the ratio of the residuals to the measured organics.

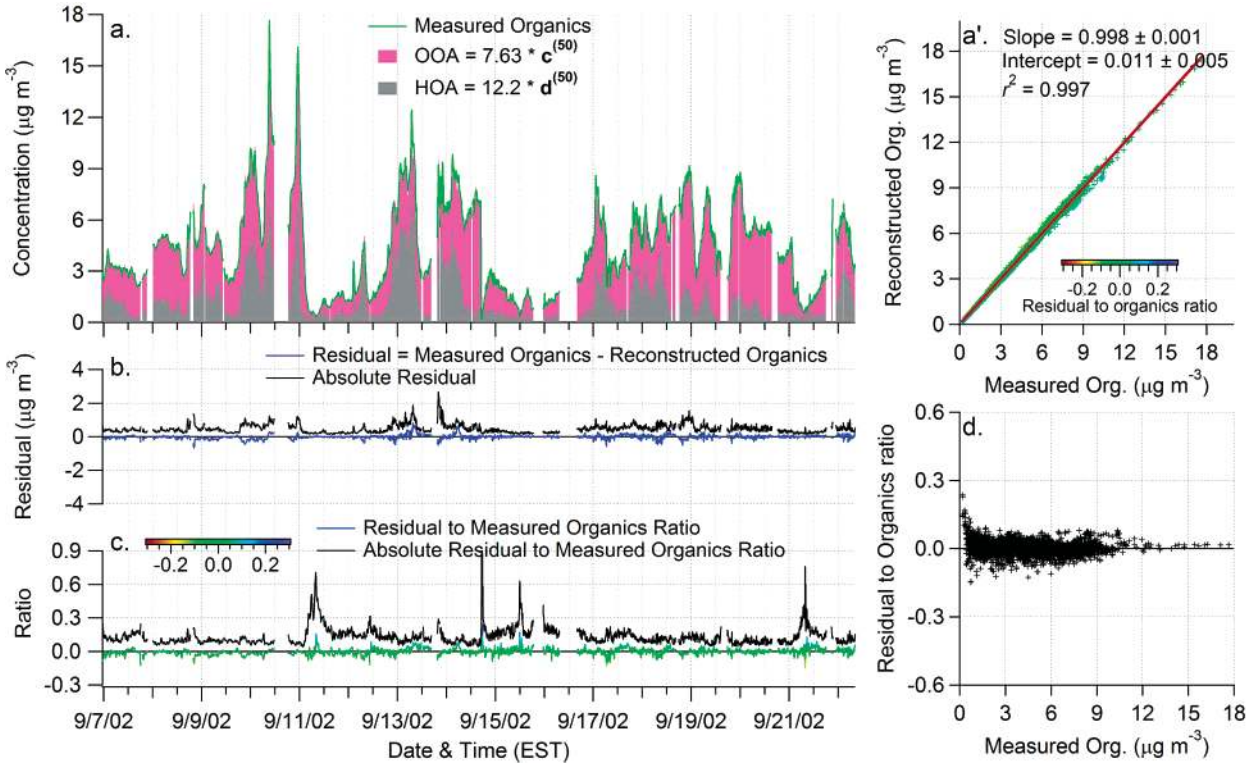

FIGURE 5. Results of algorithm 2 after 50 iterations: (a) time series of the measured organic mass concentration and HOA and OOA estimates (OOA is stacked on top of HOA); (a′) the scatter plot and linear fit (red line) between measured and reconstructed (= HOA + OOA) organic values; (b) variations of the residual of the fit (= measured − HOA − OOA) and the absolute residual (see section entitled "Calculations of Reconstructed Matrix and Residuals" for calculation) as a function of time; (c) time series of the ratio of the residual to the measured organic concentration; and (d) the scatter plot between the residuals and measured organic concentration. (a′) and (c) are colored by the ratio of the residuals to the measured organics.

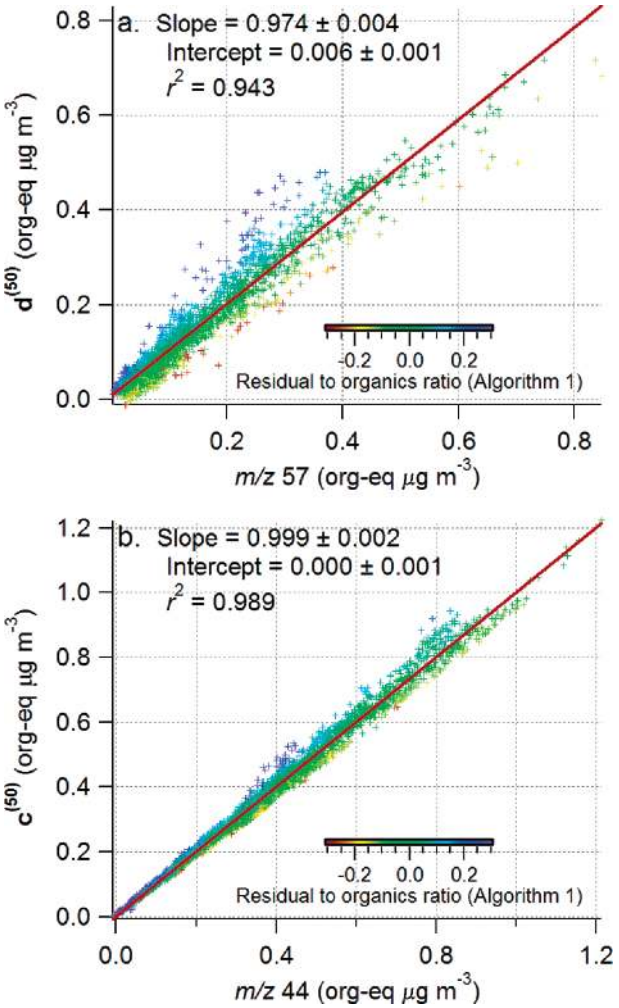

FIGURE 6. Scatter plots of (a) the d vector calculated using algorithm 2 after 50 iterations vs org$_{57}$; and (c) the c vector calculated using algorithm 2 after 50 iterations vs org$_{44}$. The red line is the least-squares linear fit.

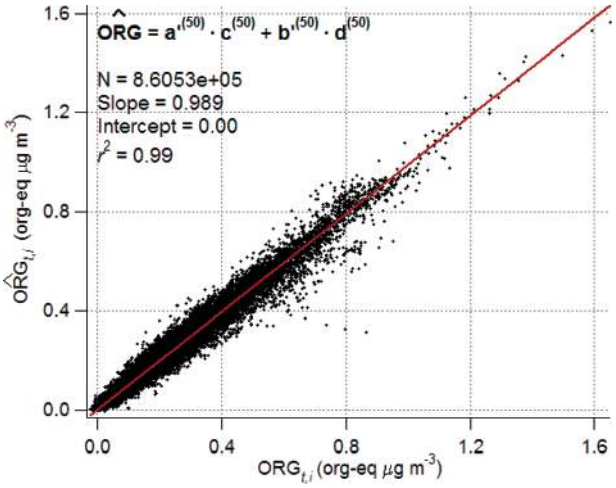

FIGURE 7. Scatter plot that compares reconstructed organic mass spectral signal intensities using algorithm 2 after 50 iterations ($\hat{ORG}_{t,i}$, eq 13) with the measured ones ($ORG_{t,i}$). $ORG_{t,i}$ and $\hat{ORG}_{t,i}$ are the tth row and the ith column elements of measured organic matrix (ORG) and reconstructed matrix ($\hat{ORG}$), respectively. See section entitled "Notation" for details on notation. The red line is the least-squares linear fit.

Note that m/z's 55 ($C_4H_7^+$) and 43 ($C_3H_7^+$) are two other prominent peaks in the AMS mass spectra of combustion exhausts and generally at intensities slightly higher than that of m/z 57 (*41, 44, 51, 55, 62*). Yet, m/z 57 is likely a better HOA mass spectral tracer since m/z's 55 and 43 tend to be more influenced by oxygenated organics, e.g., due to $C_3H_3O^+$ and $C_2H_3O^+$, respectively (*65*). One indication is that by comparison a relatively larger fraction of the m/z 57 signals are found to associate with the small mode particles in ambient air (*51, 62*). Further evidence is based on the Pearson's r values of the correlations of NO_x, CO, and SO_4^{2-} with each individual m/z's (Figure 2). Compared to those of m/z 57 ($r^2_{m/z57\ vs\ CO} = 0.75$, $r^2_{m/z57\ vs\ NOx} = 0.83$) both m/z 55 and m/z 43 show lower r values with NO_x and CO ($r^2_{m/z55\ vs\ CO} = 0.65$, $r^2_{m/z55\ vs\ NOx} = 0.72$, $r^2_{m/z43\ vs\ CO} = 0.54$, $r^2_{m/z43\ vs\ NOx} = 0.57$; Figure 2a,b) yet somehow higher r with SO_4^{2-} (Figure 2d).

(c) Association of m/z 44 with Oxygenated Organics. According to laboratory studies, the CO_2^+ ion (m/z 44) is observed intensely in the AMS mass spectra of di- and polyacids. The spectra of monoacids and other oxygenated organic compounds, including carboxylic acids, esters, carbonyls, and alcohols, also show signals at m/z 44, although at significantly lower intensity (*50*) (and unpublished data from Philip Silva, Utah State University). This is consistent with standard electron impact (EI) mass spectra of oxygenated organics (*49*), except that the corresponding AMS spectra generally show greater fragmentation (as described above) and more pronounced m/z 44 and 18 peaks (*50*) (and unpublished data from Philip Silva, Utah State University). Small dicarboxylic acids, for example, clearly undergo decarboxylation in the AMS and produce considerable signals at m/z's 18 (H_2O^+) and 44 (CO_2^+) (*50*).

In addition to m/z 44, significant m/z 28 signals are also observed in the standard EI mass spectra of organics that contain carboxyl, carbonyl, and hydroxyl functional groups (*49*). However, the AMS mass spectra of particles are often presented without the m/z 28 peak due to the difficulty of removing the overwhelming gaseous N_2^+ signals (*40*) (see section entitled "Quantification of Particle Signal at m/z 28"). In this study, we applied a recently developed procedure (*18*) to subtract the particulate m/z 28 signals from the AMS P-TOF data and compared them to the m/z 44 signals (Figure 3). Good correlations are observed between these two m/z's in signal intensity ($r^2 = 0.71$; Figure 3a) as well as in size distributions (e.g., Figure 3c), despite the comparatively noisier signals resulting from larger background subtraction at m/z 28 (see section entitled "Quantification of Particle Signal at m/z 28"). These findings, together with the observations that m/z 44 signals progressively increase during SOA formation according to smog chamber studies (*66, 67*) and that the relative intensity of m/z 44 signal increases almost linearly with the O:C ratio of a range of organic molecules (*50*) (and personal communication of Philip Silva, Utah State University), indicate a strong association of m/z 44 with oxygenated organic compounds in aerosols.

Note that although amino compounds may produce significant m/z 44 ($C_2H_6N^+$) and m/z 28 (CH_2N^+) peaks as well (*65*), these compounds are unlikely to have made significant contributions to the m/z's 28 and 44 signals observed in Pittsburgh particles. For example, the mass spectra from this study do not show obvious $C_nH_{2n+1}NH^+$ ion series pattern, which is characteristic of alkylamines (*65*) (e.g., the intensities of m/z 58 and m/z 72 signals are 1−2 orders of magnitude lower than that of m/z 44) (*18*) and m/z 30 appears to be mostly associated with NO_3^- (i.e., being NO^+ rather than $CH_2NH_2^+$) (*49*). This conclusion is consistent with findings from previous studies that amino compounds are generally a minor component of atmospheric fine particle mass (*68*−*72*). In addition, the relative intensity of m/z 44 to m/z 43 signals is ~1:1 for Pittsburgh aerosols (*18*) and thus rules out the possibility of a significant fraction of

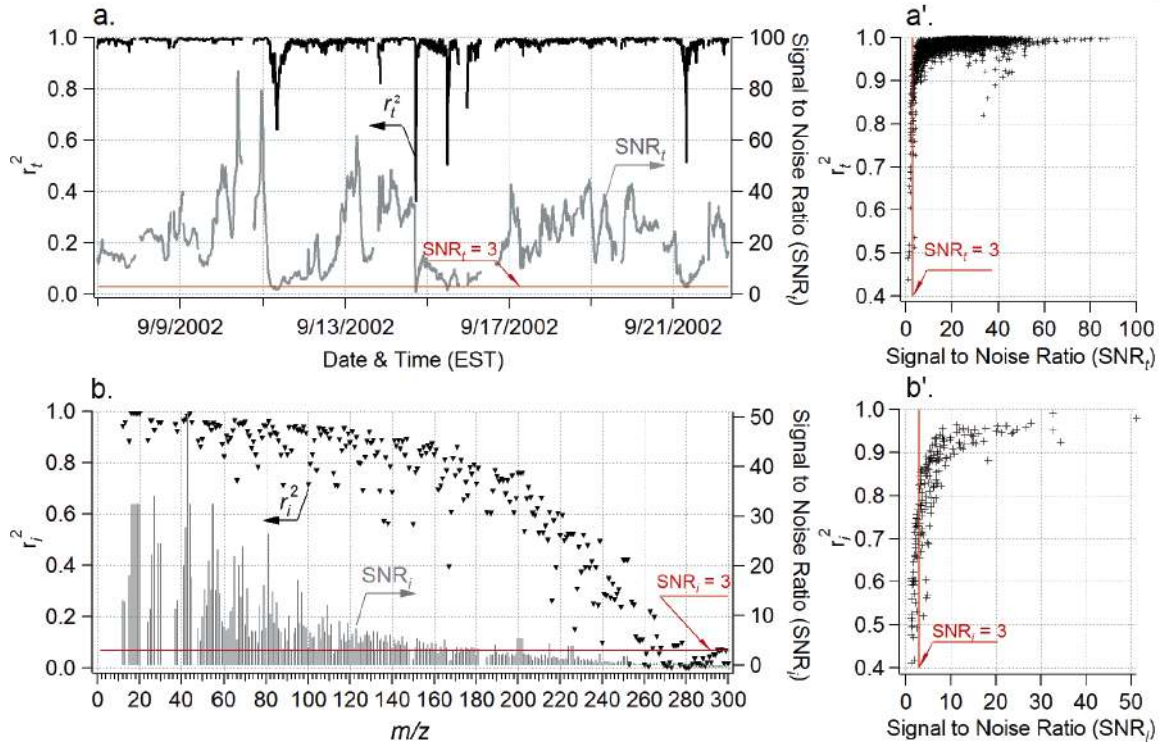

FIGURE 8. Output of the linear covariance analysis that compares the reconstructed organic mass spectral data based on algorithm 2 after 50 iterations with the measured data. (a) Variations of r_t^2 and SNR_t as a function of time; (a′) the scatter plot that compares r_t^2 vs SNR_t; (b) variations of r_i^2 and SNR_i as a function of m/z; and (b′) the scatter plot that compares r_i^2 vs SNR_i. r_t^2 is the r^2 of the correlation between the organic mass spectrum measured at time t (i.e., org_t′) and the corresponding reconstructed spectrum ($o\hat{r}g_t$′). SNR_t is the ratio of the total measured organic signal to the detection limit for organic concentration measurement (D.L. = 0.15 μg m^{-3}). r_i^2 is the r^2 of the correlation between the measured time series of organic signal at m/z = i (i.e., org_i) and the corresponding reconstructed time series (i.e., $o\hat{r}g_i$). SNR_i is the average signal-to-noise ratio for organic fragment $m/z = i$. See section entitled "Notation" for notation. Note that the reason that r_i^2's of m/z's 16, 17, 18, and 20 are the same as that of m/z 44 is that these signals were set to proportional to the organic signals at m/z 44 in the current organic analysis procedure (see section entitled "Data Preparation").

the m/z 44 signals being $^{13}C^{12}C_2H_7^+$, which is expected from alkyl chains (*65*).

In summary, m/z 57 and m/z 44 appear to be valid first-order mass spectral tracers for combustion-related hydrocarbon-like organic aerosols (HOA) and oxygenated organic aerosols (OOA), respectively. Note that m/z 44 is linked to the more broadly defined OOA, instead of secondary organic aerosols (SOA) because aged POA (*73*−*76*) and oxygenated organic species from primary emissions (*77*) may be part of this component. Biomass burning aerosols, for example, often contain significant amounts of oxygenated organic compounds as a result of oxidation in the burning process or due to burning of cellulose (*1*, *78*−*81*). Oxygenated organic compounds may also be directly emitted from vehicles, but their mass fraction is very low (a few percent or less of the total organic mass in the vehicle exhaust) (*77*) and thus make a very small contribution to the m/z 44 signal. Nevertheless, given the good correlations between m/z 44 and sulfate in size distribution and mass concentration, a significant fraction of the OOA in Pittsburgh appears to be SOA.

Apportionment of Pittsburgh Organic Mass Spectral Data. We first attempted to reconstruct the mass concentrations of total organics based on a linear combination of m/z's 44 and 57—the first-order tracers for two major organic aerosol components. Application of the first step of algorithm 1 (eq 4) yields $a = 7.6$ and $b = 12.3$, which are multiplied with the org-eq concentrations of m/z's 44 and 57, respectively, to give estimates of OOA (= 7.6 · m/z 44) and HOA (= 12.3 · m/z 57; Figure 4a). Excellent agreement is observed between the measured and reconstructed organic concentrations (= HOA + OOA), with a linear regression slope (S) = 0.99, intercept (I) = −0.01, and r^2 = 0.97 (Figure 4a′). The ratio of the residual to the measured organics concentrations varies from −0.61 to 0.58 with an average value of 0.02. The average ratio of the absolute residual to concentration is 0.08 (Figure 4c).

As shown in Figure 4d, although high residual-to-organic-ratios are generally associated with low organic concentrations, periods with high residual-to-organic-ratios also present when the organics loading is high. There are two possible reasons to explain these deviations: (1) m/z's 44 and 57 are not perfect HOA and OOA tracers; and (2) particles from these periods may contain other organic components that are not well represented by the HOA and OOA categories. The former possibility may be due to m/z 44 containing some contributions from organic particles from primary sources, such as the isotopic peak of m/z 43 ($^{13}C^{12}C_2H_7^+$), oxygenated species in vehicle emissions (*77*), and oxidized primary organic aerosols, or m/z 57 may be produced by some oxygenated organic species such as long chain alcohols or acids (see section entitled "Identification of Mass Spectral Tracers for Hydrocarbon-like and Oxygenated Organics").

We therefore used algorithm 2 (eq 11; section entitled "Mathematical Formulation") to mathematically "distill" the time series and component mass spectra of HOA and OOA. During the iterations, we observed modest improvement in χ^2's and r^2's of the fits, but the trends of these figures-of-merit quickly stabilize after only 3 iterations (i.e., $n = 3$ in eq 11). The comparisons between the improved OOA and HOA spectral tracers after 50 iterations (i.e., $\mathbf{c}^{(50)}$ and $\mathbf{d}^{(50)}$) vs $\mathbf{org}_{44}$ and $\mathbf{org}_{57}$ vectors, respectively, are shown in Figure 6. There is a very high similarity between $\mathbf{c}^{(50)}$ and $\mathbf{org}_{44}$

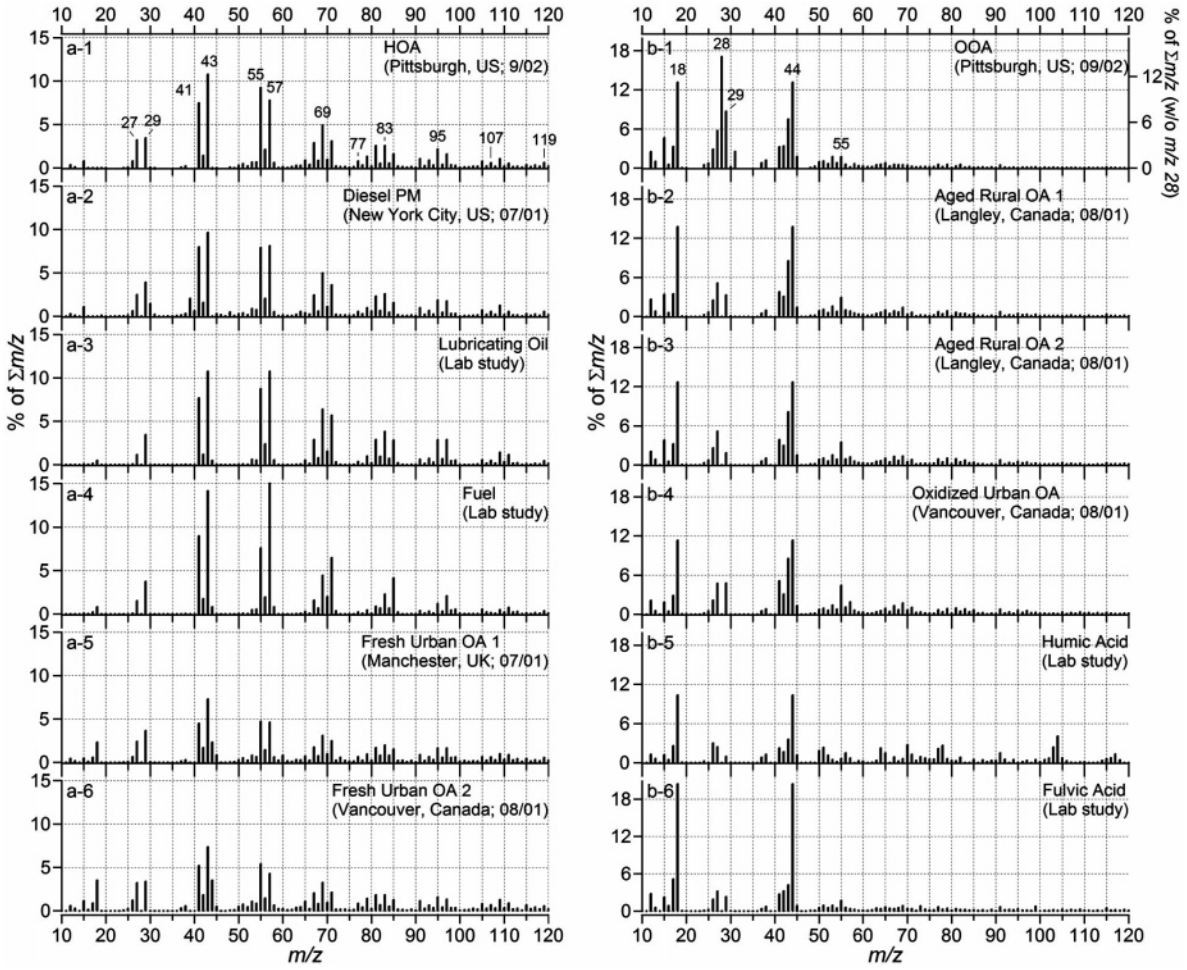

FIGURE 9. AMS mass spectra of (a-1) Pittsburgh HOA component, (a-2) diesel bus exhaust (*55*), (a-3) lubricating oil (*55*), (a-4) diesel fuel (*55*), (a-5) fresh organic aerosol components from Manchester, U.K. (*41*), (a-6) fresh organic aerosol components from Vancouver, Canada (*41*), (b-1) Pittsburgh OOA components (the *m/z* 28 peak was manually added; see section), (b-2) and (b-3) aged organic aerosols from Langley, Canada (*41*), (b-4) oxidize organic aerosols from Vancouver, Canada (*41*), (b-5) humic acid (*50*), and (b-6) fulvic acid (*50*). Sampling times and locations for these mass spectra are marked. The unit of the mass spectra is percent intensity (% of $\Sigma m/z_i$), i.e., the contribution of each peak to the total signal (not including *m/z* 28 for (b-1)) in the corresponding mass spectrum. The right *y*-axis of (b-1) indicates the percent intensity of OOA when the *m/z* 28 peak is included.

($S = 0.999$; $I = 0$; $r^2 = 0.989$). The correlation between $\mathbf{d}^{(50)}$ and $\mathbf{org}_{57}$ is slightly lower ($S = 0.974$; $I = 0$; $r^2 = 0.943$). In addition, the biggest discrepancies between $\mathbf{d}^{(50)}$ and $\mathbf{org}_{57}$ are observed when the reconstructed organic mass concentrations using algorithm 1 show the largest disagreements with the measured values. These results suggest that while it is valid to use m/z 57 as a HOA tracer the contribution of m/z 57 to the mass spectra of HOA is somewhat variable across sources and/or time periods.

The coefficients from algorithm 2 after 50 iterations (eq 11), i.e., $a^{(50)} = 7.63$ and $b^{(50)} = 12.2$ (Figure 5a), are very similar to those from algorithm 1. However, significant improvements in the fit of the total organic concentration are observed (Figure 5a,d), indicating a fraction of the residual in algorithm 1 is due to the imperfect correlation between the m/z tracers and HOA and OOA mass, especially between m/z 57 and HOA. Figure 5c,d shows that the residual-to-organic ratio is almost always below 10%. The values of the absolute residues between measured and reconstructed values (eq 14) range from 0.13 to 2.7 μg m^{-3} (average = 0.48 μg m^{-3}). Since on average the total absolute signal in an organic mass spectrum of particle-free air is 0.25 μg m^{-3}, this value sets the lower limit of whether an absolute residue is statistically different from noise. The absolute residue generally correlates with the mass concentration of organics, which is consistent with the expected increase in the noise with the magnitude of the measurement. However, there are periods when reconstructed organic values (from algorithm 2) show differences with the measured values and the absolute residuals are relatively significant. It is likely that particles from these periods contain a small fraction of the mass from organic components that are not well represented by the HOA and OOA categories (e.g. biomass burning or meat cooking). It is also possible that the mass spectra of the major components undergo small variations during the study.

We subsequently reconstruct the entire organic matrix ($\mathbf{O\hat{R}G}$) based on $\mathbf{a'}^{(50)}$, $\mathbf{b'}^{(50)}$, $\mathbf{c}^{(50)}$, and $\mathbf{d}^{(50)}$ (eqs 12 and 13). Shown in Figure 7 is the good correlation between the reconstructed ($\hat{ORG}_{t,i}$) and the measured mass spectral data ($ORG_{t,i}$). For a sample size of 8.6×10^5, the linear regression fit yields an r^2 of 0.99 ($S = 0.99$ and $I \approx 0$). This same plot also reveals a small population of data points that significantly depart from the 1:1 line. Since they were observed during the periods that show the largest discrepancies between measured and reconstructed total organic concentrations (Figure 5d), it supports the hypothesis that during certain time periods additional components are required to fully account for the variance in the mass spectral signals. However, the overall contribution of the additional components to the total organic signal appears to be small for this Pittsburgh data set.

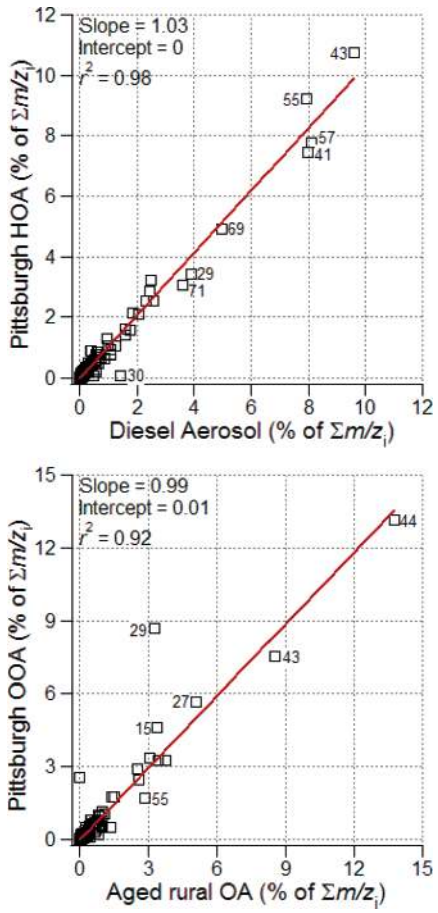

FIGURE 10. Scatter plots comparing the mass spectrum of (a) derived HOA from Pittsburgh vs fresh diesel bus exhaust aerosols sampled during New York vehicle chase study (*55*) and (b) derived OOA for Pittsburgh vs aged rural organic aerosols sampled from Vancouver, Canada (*41*). The red line is the least-squares linear fit. Intercepts for both plots are close to zero and thus not shown. *Y* axes are in percent intensity (% of Σ*m/z*), i.e., the contribution of each peak to the total signal in the corresponding mass spectrum. Values marked adjacent to the data points are the corresponding *m/z*'s.

Note that although not shown here, we were able to reproduce 98% of the variance in the organic spectral data by using algorithm 1 only. In addition, as will be discussed in section entitled "Implications", the extracted HOA and OOA mass spectra from algorithm 1 also changed little during the iteration (Figure 12). In other words, despite its simplicity, algorithm 1 has demonstrated the capability to successfully capture most of the variance in the time and m/z-resolved AMS organic data over a period of 16 days in a major urban area and thus highlights its usefulness for ambient aerosol studies.

Linear Covariance Analysis. We performed a series of linear covariance analyses between the organic mass spectral data and the results of algorithm 2 after 50 iterations, in an attempt to systematically evaluate the performance of this method. Figure 8a shows the time series of r^2_t (N_t = 3199) between measured and reconstructed mass spectra, together with the signal-to-noise ratios (SNR_t) for the corresponding mass concentration measurements. SNR_t were calculated as the ratio of the measured organic mass concentration during a time step to the average detection limit (= 0.15 μg m^{-3}) of the AMS measurement for organics during this campaign (*18*). SNR > 3 is a standard criterion to distinguish the signal from noise.

As shown in Figure 8a,a′, the r^2_t values are generally higher than 0.9. Lower r^2_t values are observed but mainly associate with very low SNR_t during periods when the organic mass concentrations are very low. However, there is a small packet of data (e.g., 19:45−20:45 on September 13th, 2002) with high SNR_t but relatively low r^2_t (although still > 0.8; Figure 8a′). Again, particles from these lower r^2_t but high SNR_t periods likely contain significant contributions from components other than the HOA and OOA extracted using these methods.

We then performed the same covariance analysis along the other dimension of the organic matrix. Figure 8b shows the r-squares for the correlation between the time series of measured and reconstructed m/z signal intensities, i.e., r^2_i as a function of m/z (N_i = 270), together with the average signal-to-noise ratios of each m/z over the entire period (SNR_i). Similar to the results for r^2_t, there is a general trend for the r^2_i values to be higher for the m/z channels that have higher signal-to-noise ratios. r^2_i's at m/z > 260 are close to zero since these m/z channels contain extremely low signals and are almost entirely noise. On the other hand, several m/z channels, such as m/z's 60, 75, 101, and 169, show good SNR_i (> 6) but relatively low r^2_i (<0.85), possibly due to association with other components. In principle, the r-square plots shown in Figure 8 provide an overview of the performance of the fit model we developed from this study. This analysis may be used as guidance for studies with data from other locations and to help resolve more components in the particles.

The Mass Spectra of HOA and OOA. Algorithms 1 and 2 also allow us to derive a first and a refined approximation, respectively, to the component mass spectra of HOA and OOA (eqs 6 and 7). The word "component" is used since these two mass spectra are expected to represent mixtures of many individual organic species associated with the same sources (or group of sources) and atmospheric processes, rather than individual species or functional groups. As shown in Figure 9a-1, the extracted mass spectrum of HOA demonstrates prominent ion series for hydrocarbons, which are major components identified in diesel and gasoline engine exhaust particles, and fuel and lubricating oil, e.g., the $C_nH_{2n+1}^+$ sequence (m/z 29, 43, 57, 71, 85...) that is particularly prevalent for alkanes, the $C_nH_{2n-1}^+$ sequence (m/z 27, 41, 55, 69, 83, 97...) that can be produced from H_2 neutral loses from alkyl fragments and/or alkenes, and the $C_nH_{2n-3}^+$ sequence (m/z 67, 81, 95, 107...) that can arise from cycloalkanes (*41, 55, 65, 82, 83*). The ion series that can be associated with aromatic species (m/z 77, 91, 105, 119) (*65*) is also observed.

The component HOA mass spectrum is remarkably similar to the AMS mass spectra of diesel bus exhaust aerosols sampled during "vehicle chasing" experiments in New York City (Figure 9a-2) (*55*). The r^2 between these two mass spectra is 0.98 (S = 1.02; I = 0.01; Figure 10a). In addition, the HOA spectrum also closely resembles those of the more volatile fraction of lubricating oil and fuel aerosols that were generated in the lab through nucleation and condensation of the vapors from hot oil or fuel (*55*) (Figure 9a-3,9a-4) and freshly emitted traffic aerosols in two urban locations—Manchester, U.K. (*62*) and Vancouver, Canada (*41*) (Figure 9a-5,9a-6).

The derived component mass spectrum of OOA (Figure 9b-1) demonstrates a starkly different fragmentation pattern than that of HOA (Figure 9a-1). First of all, the OOA mass spectrum is dominated by smaller fragments and contains very little signal at m/z > 55 (60% of the total signal is above m/z 55 for HOA vs 15% for OOA). Second, the OOA spectrum is dominated by m/z 44 (CO_2^+). The signal at m/z 18 (H_2O^+) is set equal to that of m/z 44 in the current organic analysis procedure based on laboratory studies of carboxylic and dicarboxylic acids (Philip Silva, personal communication) and since it is not possible to directly measure this signal due to interferences with particle-phase water, and with H_2O molecules arising due to the decomposition of ammonium

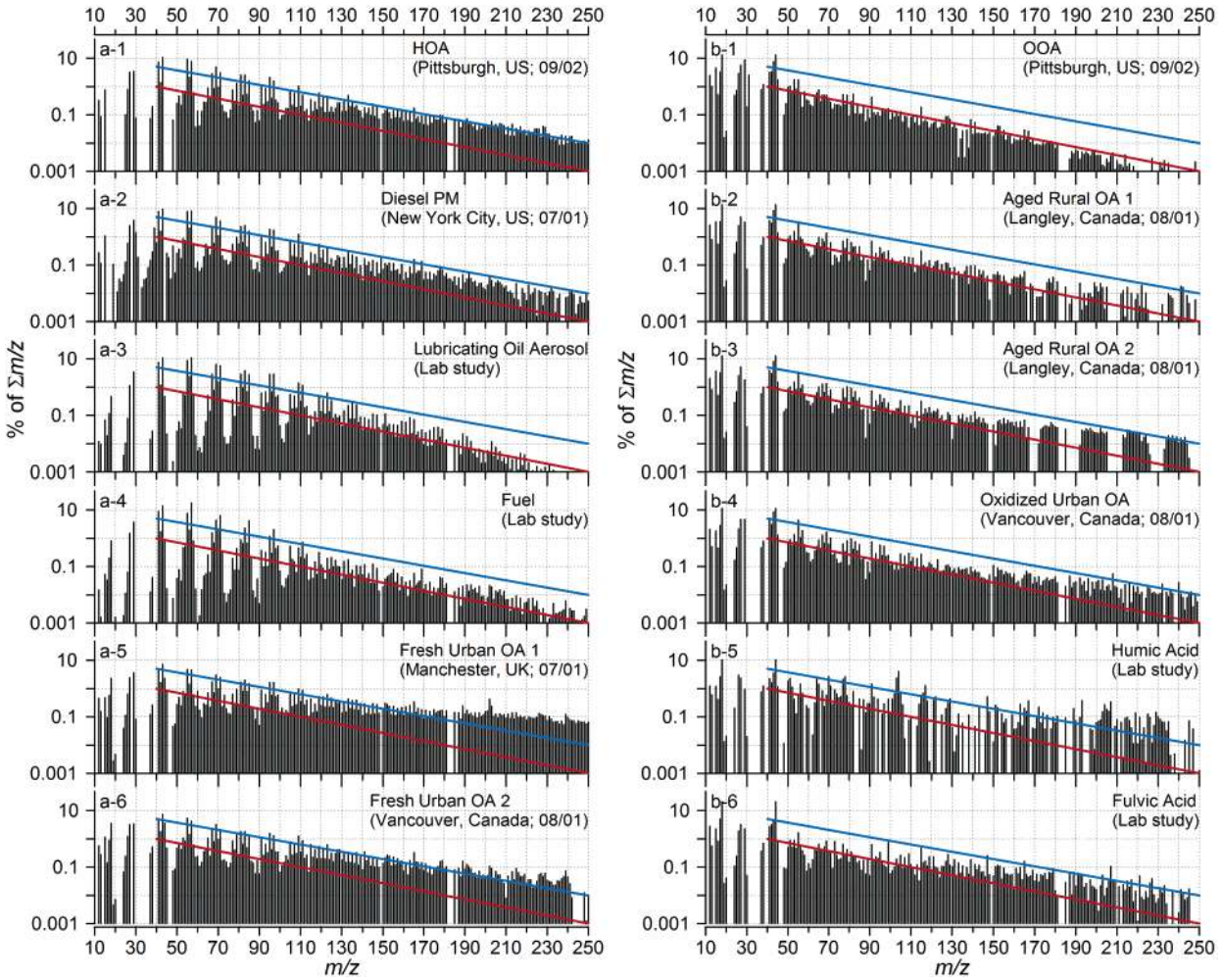

FIGURE 11. The log scale AMS mass spectra, corresponding to those shown in Figure 8. Two lines have been added to the mass spectra to guide the eye: the blue line is an approximate fit to the envelope of the *m/z* 40−250 range of the log scale mass spectra of Pittsburgh HOA and the red line to that of Pittsburgh OOA.

sulfate or sulfuric acid during their evaporation in the AMS (*40*). In addition, the OOA spectrum displays a significant m/z 45 signal ($COOH^+$), a fragment observed from carboxylic acids (*49, 50*) and that is nearly zero in the HOA spectrum (Figure 9a-1). All of these features have been observed for highly processed organic aerosols in ambient air at several locations (*18, 36, 41, 54, 62*).

The derived OOA mass spectrum demonstrates close similarity in the overall pattern with those of aged/oxidized organic aerosols in rural and urban areas (Figure 9b-2−9b-4). A linear regression between the mass spectra of OOA from this study and that of aged rural organic aerosols from Langley (the rural site of Vancouver), Canada (*41*), in particular, yields $S = 1.02$, $I = -0.01$, and $r^2 = 0.93$ (Figure 10b). In addition, the OOA mass spectrum is qualitatively similar to the AMS mass spectra of the fulvic and humic acids (*50*)—classes of highly oxygenated organic compounds that have been proposed as models of the highly oxidized organic aerosols that are ubiquitous in the atmosphere, based on their responses to analytical procedures such as proton nuclear magnetic resonance and Fourier transform infrared spectroscopy (*84*) (Figure 9b-5,9b-6).

Figure 11 shows the same set of mass spectra on a log scale, with the purpose to illustrate the differences between these mass spectra at high m/z's. Again, the difference between OOA and HOA for large m/z is dramatic. The HOA components produce at least 1 order of magnitude more signal for the high m/z fragments than the OOA components do. This is consistent with the correlations shown in Figure 2, which shows that the high m/z fragments correlated better with CO than with sulfate. Also, among all the spectra, the extracted OOA spectrum from Pittsburgh contains the least amount of high m/z fragments, suggesting that the OOA components in Pittsburgh are either relatively lower in molecular weight or more prone to fragmentation.

Finally, we compared the HOA and OOA mass spectra obtained from algorithm 1 vs those from algorithm 2 after 50 iterations (Figure 12). Only minor differences are observed, but again the changes in the HOA spectrum were larger than those in the OOA spectrum, indicating that m/z 57 is a less optimum HOA tracer than m/z 44 is for OOA. As shown in Figure 9b-1, an important change is a small m/z 57 peak that appeared in the OOA mass spectrum, which fits the patterns of the surrounding peaks on the OOA spectrum. The contribution of m/z 57 to the total signal in the OOA mass spectrum is ~0.3%. Although we expect that there should be an isotopic peak of $^{13}C_1{}^{12}C_2H_7^+$ (m/z 44) present at an abundance of 3.3% of the signal intensity of $^{12}C_3H_7^+$ (m/z 43) (*65*), the calculated m/z 44 peak in HOA remains close to zero after iteration. This is due to the very low intensity of $^{13}C_1{}^{12}C_2H_7^+$ signals (e.g., estimated org-eq concentration of $^{13}C_1{}^{12}C_2H_7^+$ in HOA is 0.005 $\mu g\ m^{-3}$), which is indistinguishable from noise.

Implications. The key result of the procedures presented here is that m/z 44 and m/z 57 are reliable AMS mass spectral "markers" which allow the quantification of HOA and OOA

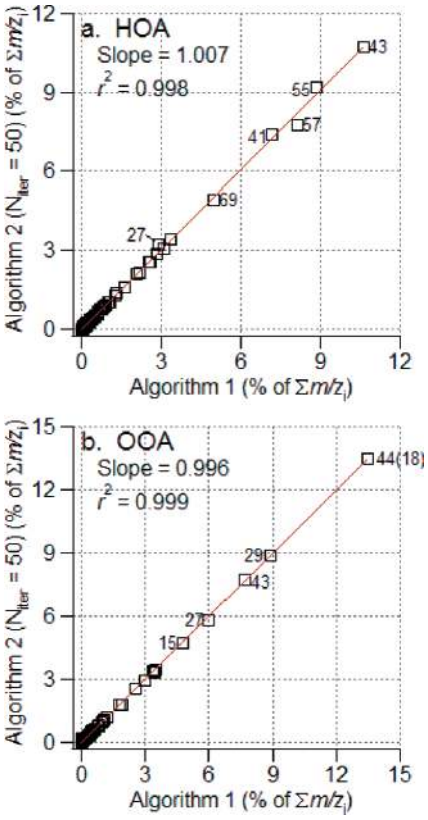

FIGURE 12. Scatter plots comparing the mass spectra of (a) Pittsburgh HOA components and (b) Pittsburgh OOA components obtained by algorithm 2 after 50 iterations to those obtained by algorithm 1. The red line is the least-squares linear fit. Intercepts for both plots are close to zero and thus not shown. *Y* axes are in percent intensity (% of Σ*m*/*z*), i.e., the contribution of each peak to the total signal in the corresponding mass spectrum. Values marked adjacent to the data points are the corresponding *m*/*z*'s.

and the extraction of mass spectra that can be interpreted chemically. Algorithm 1 yields most of the information while providing the "first guess" for algorithm 2 which is more quantitative. This simple linear superposition model of only two components with constant mass spectra reduces the complexity of aerosol mass spectrometry data by a factor of ~150 while accounting for most of the variance in the concentrations and mass spectra of organic aerosols in a major urban area for a period of 16 days. In addition, the mass spectra of the two components are remarkably invariant in time. This contrasts with other apportionment studies using molecular tracers that identify large numbers of sources, e.g., ref *23*, and may be due to multiple combustion related sources being lumped under HOA in this study, if their bulk chemical compositions (as opposed to their tracer concentrations) are quite similar. In other words, we believe that underneath the apparent simplicity of each of the two components there likely lies considerable complexity—e.g., compounds that have similar temporal variations or similar mass spectra are likely grouped together. Aerosols having significantly different sources/precursors, e.g., biogenic vs anthropogenic SOA, or traffic vs power plant emission POA, may not be discriminated by the technique presented here. We plan to address this point by further developing the technique so that more components can be extracted and by comparing with other source apportionment techniques for simultaneously collected data as part of a currently funded project.

In a separate paper we interpret the results obtained with the method described here (algorithm 2) in terms of the properties of HOA and OOA in the Pittsburgh Supersite data set, including their diurnal profiles, and compare to previous results at this and other locations. We also derive the highly time-resolved size distributions of HOA and OOA by using a procedure based on these results and explore the implications of the time series, diurnal profiles, and size distributions on the sources and process responsible for the observed HOA and OOA (Zhang et al., in preparation for *Atmos. Chem. Phys.*).

Acknowledgments

This research was partially supported by EPA STAR Grants R831080 and RD832161010, by NSF CAREER grant ATM 0449815, and by NASA Grant NNG04GA67G. Although this work has been partly funded by EPA, it has not been subjected to the Agency's review and therefore does not necessarily reflect the views of the Agency and no official endorsement should be inferred. The authors thank Dr. Beth Wittig (CMU) for gas phase and meteorology data, Drs. R. Subramanian, Juan Cabada-Amaya, and Allen Robinson (CMU), Andrea Polidori, and Dr. Barbara Turpin (Rutgers University) for EC data. The authors also thank Dr. Meinrat O. Andreae (Max Planck Institute for Chemistry) and one anonymous reviewer for their constructive suggestions on organic aerosol terminology. Finally we thank the Jimenez group and the AMS community for many helpful discussions.

Supporting Information Available

Figures S1−S10. This material is available free of charge via the Internet at http://pubs.acs.org.

Literature Cited

(1) Jacobson, M. C.; Hansson, H. C.; Noone, K. J.; Charlson, R. J. Organic atmospheric aerosols: Review and state of the science. *Rev. Geophys.* **2000**, *38*, 267−294.

(2) Seinfeld, J. H.; Pankow, J. F. Organic atmospheric particulate material. *Annu. Rev. Phys. Chem.* **2003**, *54*, 121−140.

(3) Andreae, M. O.; Crutzen, P. J. Atmospheric aerosols: Biogeochemical sources and role in atmospheric chemistry. *Science* **1997**, *276*, 1052−1058.

(4) Cass, G. R.; Hughes, L. A.; Bhave, P.; Kleeman, M. J.; Allen, J. O.; Salmon, L. G. The chemical composition of atmospheric ultrafine particles. *Philos. Trans. R. Soc. London Ser. A-Math. Phys. Eng. Sci* **2000**, *358*, 2581−2592.

(5) Rogge, W. F.; Mazurek, M. A.; Hildemann, L. M.; Cass, G. R.; Simoneit, B. R. T. Quantification of urban organic aerosols at a molecular level − Identification, abundance and seasonal variation. *Atmos. Environ. A* **1993**, *27*, 1309−1330.

(6) NARSTO. *Particulate Matter Science for Policy Makers: A NARSTO Assessment*; EPRI 1007735; 2003.

(7) Turpin, B. J.; Saxena, P.; Andrews, E. Measuring and simulating particulate organics in the atmosphere: problems and prospects. *Atmos. Environ.* **2000**, *34*, 2983−3013.

(8) IPCC. *Climate Change 2001: The Scientific Basis, Contribution of Working Group I to the Third Assessment Report of the Intergovernmental Panel on Climate Change*; Houghton, J. T., et al., Ed.; Cambridge University Press: New York, 2001.

(9) Watson, J. G. Visibility: Science and regulation. *J. Air Waste Manage. Assoc.* **2002**, *52*, 628−713.

(10) Jang, M. S.; Czoschke, N. M.; Lee, S.; Kamens, R. M. Heterogeneous atmospheric aerosol production by acid-catalyzed particle-phase reactions. *Science* **2002**, *298*, 814−817.

(11) Claeys, M.; Wang, W.; Ion, A. C.; Kourtchev, I.; Gelencser, A.; Maenhaut, W. Formation of secondary organic aerosols from isoprene and its gas-phase oxidation products through reaction with hydrogen peroxide. *Atmos. Environ.* **2004**, *38*, 4093−4098.

(12) Blando, J. D.; Turpin, B. J. Secondary organic aerosol formation in cloud and fog droplets: a literature evaluation of plausibility. *Atmos. Environ.* **2000**, *34*, 1623−1632.

(13) Corrigan, C. E.; Novakov, T. Cloud condensation nucleus activity of organic compounds: a laboratory study. *Atmos. Environ.* **1999**, *33*, 2661−2668.

(14) Mircea, M.; Facchini, M. C.; Decesari, S.; Fuzzi, S.; Charlson, R. J. The influence of the organic aerosol component on CCN supersaturation spectra for different aerosol types. *Tellus Ser. B−Chem. Phys. Meteorol.* **2002**, *54*, 74−81.

(15) Kerminen, V. M.; Virkkula, A.; Hillamo, R.; Wexler, A. S.; Kulmala, M. Secondary organics and atmospheric cloud condensation nuclei production. *J. Geophys. Res., [Atmos.]* **2000**, *105*, 9255−9264.
(16) Cruz, C. N.; Pandis, S. N. A study of the ability of pure secondary organic aerosol to act as cloud condensation nuclei. *Atmos. Environ.* **1997**, *31*, 2205−2214.
(17) Kavouras, I. G.; Stephanou, E. G. Particle size distribution of organic primary and secondary aerosol constituents in urban, background marine, and forest atmosphere. *J. Geophys. Res., [Atmos.]* **2002**, *107*.
(18) Zhang, Q.; Canagaratna, M. C.; Jayne, J. T.; Worsnop, D. R.; Jimenez, J. L. Time and size-resolved chemical composition of submicron particles in Pittsburgh − Implications for aerosol sources and processes. *J. Geophys. Res.* **2005**, *110*, doi:10.1029/2004JD004649.
(19) Russell, A.; Dennis, R. NARSTO critical review of photochemical models and modeling. *Atmos. Environ.* **2000**, *34*, 2283−2324.
(20) Strader, R.; Lurmann, F.; Pandis, S. N. Evaluation of secondary organic aerosol formation in winter. *Atmos. Environ.* **1999**, *33*, 4849−4863.
(21) Pandis, S. N.; Harley, R. A.; Cass, G. R.; Seinfeld, J. H. Secondary organic aerosol formation and transport. *Atmos. Environ. A* **1992**, *26*, 2269−2282.
(22) Cass, G. R. Organic molecular tracers for particulate air pollution sources. *TrAC, Trends Anal. Chem.* **1998**, *17*, 356−366.
(23) Schauer, J. J.; Rogge, W. F.; Hildemann, L. M.; Mazurek, M. A.; Cass, G. R. Source apportionment of airborne particulate matter using organic compounds as tracers. *Atmos. Environ.* **1996**, *30*, 3837−3855.
(24) Zheng, M.; Cass, G. R.; Schauer, J. J.; Edgerton, E. S. Source apportionment of $PM_{2.5}$ in the southeastern United States using solvent-extractable organic compounds as tracers. *Environ. Sci. Technol.* **2002**, *36*, 2361−2371.
(25) Turpin, B. J.; Huntzicker, J. J. Secondary formation of organic aerosol in the Los Angeles basin: A descriptive analysis of organic and elemental carbon concentrations. *Atmos. Environ. Part A General Topics* **1991**, *25*, 207−215.
(26) Turpin, B. J.; Huntzicker, J. J. Identification of secondary organic aerosol episodes and quantitation of primary and secondary organic aerosol concentrations during SCAQS. *Atmos. Environ.* **1995**, *29*, 3527−3544.
(27) Castro, L. M.; Pio, C. A.; Harrison, R. M.; Smith, D. J. T. Carbonaceous aerosol in urban and rural European atmospheres: estimation of secondary organic carbon concentrations. *Atmos. Environ.* **1999**, *33*, 2771−2781.
(28) Cabada, J. C.; Pandis, S. N.; Robinson, A. L. Sources of atmospheric carbonaceous particulate matter in Pittsburgh, Pennsylvania. *J. Air Waste Manage. Assoc.* **2002**, *52*, 732−741.
(29) Cabada, J. C.; Pandis, S. N.; Subramanian, R.; Robinson, A. L.; Polidori, A.; Turpin, B. Estimating the secondary organic aerosol contribution to $PM_{2.5}$ using the EC tracer method. *Aerosol Sci. Technol.* **2004**, *38(S1)*, 140−155.
(30) Malinowski, E. R. *Factor Analysis in Chemistry*, 3rd ed.; Wiley-Interscience: New York, 2002.
(31) Paatero, P.; Tapper, U. Positive matrix factorization: A non-negative factor model with optimal utilization of error estimates of data values. *Environmetrics* **1994**, *5*, 111−126.
(32) Henry, R. C.; Lewis, C. W.; Collins, J. F. Vehicle-related hydrocarbon source composition from ambient data: The GRACE/SAFER method. *Environ. Sci. Technol.* **1994**, *28*, 823−832.
(33) Schauer, J. J.; Cass, G. R. Source apportionment of wintertime gas-phase and particle-phase air pollutants using organic compounds as tracers. *Environ. Sci. Technol.* **2000**, *34*, 1821−1832.
(34) Fine, P. M.; Chakrabarti, B.; Krudysz, M.; Schauer, J. J.; Sioutas, C. Diurnal variations of individual organic compound constituents of ultrafine and accumulation mode particulate matter in the Los Angeles Basin. *Environ. Sci. Technol.* **2004**, *38*, 1296−1304.
(35) Schauer, J. J.; Fraser, M. P.; Cass, G. R.; Simoneit, B. R. T. Source reconciliation of atmospheric gas-phase and particle-phase pollutants during a severe photochemical smog episode. *Environ. Sci. Technol.* **2002**, *36*, 3806−3814.
(36) Jimenez, J. L.; Jayne, J. T.; Shi, Q.; Kolb, C. E.; Worsnop, D. R.; Yourshaw, I.; Seinfeld, J. H.; Flagan, R. C.; Zhang, X.; Smith, K. A.; Morris, J. W.; Davidovits, P. Ambient aerosol sampling with an Aerosol Mass Spectrometer. *J. Geophys. Res.* **2003**, *108*, 8425, doi: 8410:1029/2001JD001213.
(37) Jimenez, J. L.; Bahreini, R.; Cocker, D. R.; Zhuang, H.; Varutbangkul, V.; Flagan, R. C.; Seinfeld, J. H.; O'Dowd, C.; Hoffmann, T. New particle formation from photooxidation of diiodomethane (CH_2I_2). *J. Geophys. Res., [Atmos.]* **2003**, *108*, 4318, doi: 4310.1029/2002JD002452.
(38) Jayne, J. T.; Leard, D. C.; Zhang, X.; Davidovits, P.; Smith, K. A.; Kolb, C. E.; Worsnop, D. R. Development of an aerosol mass spectrometer for size and composition analysis of submicron particles. *Aerosol. Sci. Technol.* **2000**, *33*, 49−70.
(39) Allan, J. D.; Jimenez, J. L.; Williams, P. I.; Alfarra, M. R.; Bower, K. N.; Jayne, J. T.; Coe, H.; Worsnop, D. R. Quantitative sampling using an Aerodyne Aerosol Mass Spectrometer. Part 1: Techniques of data interpretation and error analysis. *J. Geophys. Res., [Atmos.]* **2003**, *108*, 4090, doi: 4010.1029/2002JD002358.
(40) Allan, J. D.; Delia, A. E.; Coe, H.; Bower, K. N.; Alfarra, M. R.; Jimenez, J. L.; Middlebrook, A. M.; Drewnick, F.; Onasch, T. B.; Canagaratna, M. R.; Jayne, J. T.; Worsnop, D. R. A generalised method for the extraction of chemically resolved mass spectra from Aerodyne aerosol mass spectrometer data. *J. Aerosol Sci.* **2004**, *35*, 909−922, doi: 910.1016/j.jaerosci.2004.1002.1007.
(41) Alfarra, M. R.; Coe, H.; Allan, J. D.; Bower, K. N.; Boudries, H.; Canagaratna, M. R.; Jimenez, J. L.; Jayne, J. T.; Garforth, A.; Li, S.-M.; Worsnop, D. R. Characterization of urban and regional organic aerosols in the lower Fraser Valley using two Aerodyne Aerosol Mass Spectrometers. *Atmos. Environ.* **2004**, 5745−5758.
(42) Drewnick, F.; Schwab, J. J.; Hogrefe, O.; Peters, S.; Husain, L.; Diamond, D.; Weber, R.; Demerjian, K. L. Intercomparison and evaluation of four semi-continuous $PM_{2.5}$ sulfate instruments. *Atmos. Environ.* **2004**, *37*, 3335−3350.
(43) Drewnick, F.; Schwab, J. J.; Jayne, J. T.; Canagaratna, M.; Worsnop, D. R.; Demerjian, K. L. Measurement of ambient aerosol composition during the PMTACS-NY 2001 using an Aerosol Mass Spectrometer. Part I: Mass concentrations. *Aerosol Sci. Technol.* **2004**, *38*, 92−103.
(44) Allan, J. D.; Bower, K. N.; Coe, H.; Boudries, H.; Jayne, J. T.; Canagaratna, M. R.; Millet, D. B.; Goldstein, A. H.; Quinn, P. K.; Weber, R. J.; Worsnop, D. R. Submicron aerosol composition at Trinidad Head, California, during ITCT 2K2: Its relationship with gas-phase volatile organic carbon and assessment of instrument performance. *J. Geophys. Res., [Atmos.]* **2004**, *109*, D23S24, doi: 10.1029/2003JD004208.
(45) Liu, B. Y. H.; Ziemman, P. J.; Kittelson, D. B.; McMurry, P. H. Generating particle beams of controlled dimensions and divergence: II. experimental evaluation of particle motion in aerodynamic lenses and nozzle expansions. *Aerosol Sci. Technol.* **1995**, *22*, 314−324.
(46) Zhang, X.; Smith, K. A.; Worsnop, D. R.; Jimenez, J. L.; Jayne, J. T.; Kolb, C. E. A numerical characterization of particle beam collimation by an aerodynamic lens-nozzle system. Part I: An individual lens or nozzle. *Aerosol Sci. Technol.* **2002**, *36*, 617−631.
(47) Zhang, X.; Smith, K. A.; Worsnop, D. R.; Jimenez, J. L.; Jayne, J. T.; Kolb, C. E.; Morris, J.; Davidovits, P. Characterization of particle beam collimation: Part II Integrated aerodynamic lens-nozzle system. *Aerosol Sci. Technol.* **2004**, *38*, 619−638.
(48) Reilly, P. T. A.; Lazar, A. C.; Gieray, R. A.; Whitten, W. B.; Ramsey, J. M. The elucidation of charge-transfer-induced matrix effects in environmental aerosols via real-time aerosol mass spectral analysis of individual airborne particles. *Aerosol Sci. Technol.* **2000**, *33*, 135−152.
(49) Stein, S.; Mirokhin, Y.; Tchekhovskoi, D.; Mallard, G. *The NIST Mass Spectral Search Program for the NIST/EPA/NIH Mass Spectral Library (Version 2.0)*; The Standard Reference Data Program of NIST, 2001.
(50) Alfarra, M. R. Ph.D. Dissertation, Insights into Atmospheric Organic Aerosols Using an Aerosol Mass Spectrometer, University of Manchester, 2004.
(51) Zhang, Q.; Stanier, C. O.; Canagaratna, M. R.; Jayne, J. T.; Worsnop, D. R.; Pandis, S. N.; Jimenez, J. L. Insights into the chemistry of new particle formation and growth events in Pittsburgh based on Aerosol Mass Spectrometry. *Environ. Sci. Technol.* **2004**, *38*, 4797−4809.
(52) Takegawa, N.; Miyazaki, Y.; Kondo, Y.; Komazaki, Y.; Miyakawa, T.; Jimenez, J. L.; Jayne, J. T.; Worsnop, D. R.; Allan, J. D.; Weber, R. J. Characterization of an Aerodyne Aerosol Mass Spectrometer (AMS): Intercomparison with other aerosol instruments. *Aerosol Sci. Technol.* **2005**, in press.
(53) Canagaratna et al. Ambient Aerosol Analysis with the Aerodyne AMS in the Houston 2000 Study. *J. Geophys. Res., [Atmos.]* **2005**, manuscript in preparation.
(54) Bahreini, R.; Jimenez, J. L.; Wang, J.; Flagan, R. C.; Seinfeld, J. H.; Jayne, J. T.; Worsnop, D. R. Aircraft-based aerosol size and composition measurements during ACE-Asia using an Aerodyne

aerosol mass spectrometer. *J. Geophys. Res., [Atmos.]* **2003**, *108*, 8645, doi: 8610.1029/2002JD003226.
(55) Canagaratna, M. R.; Jayne, J. T.; Ghertner, D. A.; Herndon, S.; Shi, Q.; Jimenez, J. L.; Silva, P. J.; Williams, P.; Lanni, T.; Drewnick, F.; Demerjian, K. L.; Kolb, C. E.; Worsnop, D. R. Chase studies of particulate emissions from in-use New York city vehicles. *Aerosol Sci. Technol.* **2004**, *38*, 555−573, 510.1080/02786820490465504.
(56) Jackson, J. E. *A User's Guide to Principal Components*; John Wiley & Son, Inc.: Hoboken, NJ, 2003.
(57) Katrib, Y.; Martin, S. T.; Hung, H. M.; Rudich, Y.; Zhang, H.; Slowik, J.; Davidovits, P.; Jayne, J. T.; Worsnop, D. R. Products and mechanisms of ozone reactions with oleic acid for aerosol particles having core-shell morphologies. *J. Phys. Chem. A* **2004**, *108*, 6686−6695.
(58) Seinfeld, J. H.; Pandis, S. N. *Atmospheric Chemistry and Physics: From Air Pollution to Climate Change*; Wiley: New York, 1998.
(59) Paatero, P.; Hopke, P. K.; Begum, B. A.; Biswas, S. K. A graphical diagnostic method for assessing the rotation in factor analytical models of atmospheric pollution. *Atmos. Environ.* **2005**, *39*, 193−201.
(60) Stein, S. E.; Scott, D. R. Optimization and testing of mass-spectral library search algorithms for compound identification. *J. Am. Soc. Mass Spectrom.* **1994**, *5*, 859−866.
(61) Press: W. H.; Teukolsky, S. A.; Vetterling, W. T.; Flannery, B. P. *Numerical Recipes in C: The Art of Scientific Computing*, 2nd ed.; Cambridge University Press: Cambridge, New York, Port Chester, Melbourne, Sydney, 1992.
(62) Allan, J. D.; Alfarra, M. R.; Bower, K. N.; Williams, P. I.; Gallagher, M. W.; Jimenez, J. L.; McDonald, A. G.; Nemitz, E.; Canagaratna, M. R.; Jayne, J. T.; Coe, H.; Worsnop, D. R. Quantitative sampling using an Aerodyne Aerosol Mass Spectrometer. Part 2: Measurements of fine particulate chemical composition in two UK Cities. *J. Geophys. Res., [Atmos.]* **2003**, *108*, 4091, doi: 4010.1029/2002JD002359.
(63) Dzepina et al. Characterization of ambient aerosol in Mexico City: The organic component. *Atmos. Chem. Phys.* **2005**, manuscript in preparation.
(64) Baumgardner, D.; Raga, G.; Peralta, O.; Rosas, I.; Castro, T.; Kuhlbusch, T.; John, A.; Petzold, A. Diagnosing black carbon trends in large urban areas using carbon monoxide measurements. *J. Geophys. Res., [Atmos.]* **2002**, *107*.
(65) McLafferty, F. W.; Turecek, F. *Interpretation of Mass Spectra*; University Science Books: Mill Valley, CA, 1993.
(66) Alfarra, M. R.; Paulsen, D.; Gysel, M.; Garforth, A. A.; Dommen, J.; Prevot, A. S. H.; Worsnop, D. R.; Baltensperger, U.; Coe, H. A Mass Spectrometric study of secondary organic aerosols formed from the photooxidation of anthropogenic and biogenic precursors in a reaction chamber. *Environ. Sci. Technol.* **2004**, submitted for publication.
(67) Bahreini, R.; Keywood, M.; Ng, N. L.; Varutbangkul, V.; Gao, S.; Flagan, R. C.; Seinfeld, J. H.; Worsnop, D. R.; Jimenez, J. L. Measurements of secondary organic aerosols (SOA) from oxidation of cycloalkanes, terpenes, and *m*-xylene using the Aerodyne Aerosol Mass Spectrometer (AMS). *Environ. Sci. Technol.* **2005**, in press.
(68) Zhang, Q.; Anastasio, C. Free and combined amino compounds in atmospheric fine particles ($PM_{2.5}$) and fogwaters from Northern California. *Atmos. Environ.* **2003**, *37*, 2247−2258.
(69) Zhang, Q.; Anastasio, C.; Jimenez-Cruz, M. Water-soluble organic nitrogen in atmospheric fine particles ($PM_{2.5}$) from Northern California. *J. Geophys. Res.* **2002**, *107(D11)*, 4112, doi: 4110.1029/2001JD000870.
(70) Milne, P. J.; Zika, R. G. Amino acid nitrogen in atmospheric aerosols − Occurrence, sources and photochemical modification. *J. Atmos. Chem.* **1993**, *16*, 361−398.
(71) Cornell, S. E.; Jickells, T. D.; Thornton, C. A. Urea in rainwater and atmospheric aerosol. *Atmos. Environ.* **1998**, *32*, 1903−1910.
(72) Gorzelska, K.; Talbot, R. W.; Klemm, K.; Lefer, B.; Klemm, O.; Gregory, G. L.; Anderson, B.; Barrie, L. A. Chemical composition of the atmospheric aerosol in the troposphere over the Hudson Bay lowlands and Quebec-Labrador regions of Canada. *J. Geophys. Res., [Atmos.]* **1994**, *99*, 1763−1779.
(73) Donahue, N.; Robinson, A. Theoretical, in situ, and laboratory constraints on organic aerosol oxidation, AAAR 2004 Annual Conference, 2004.
(74) Eliason, T. L.; Gilman, J. B.; Vaida, V. Oxidation of organic films relevant to atmospheric aerosols. *Atmos. Environ.* **2004**, *38*, 1367−1378.
(75) Bertram, A. K.; Ivanov, A. V.; Hunter, M.; Molina, L. T.; Molina, M. J. The reaction probability of OH on organic surfaces of tropospheric interest. *J. Phys. Chem. A* **2001**, *105*, 9415−9421.
(76) Molina, M. J.; Ivanov, A. V.; Trakhtenberg, S.; Molina, L. T. Atmospheric evolution of organic aerosol. *Geophys. Res. Lett.* **2004**, *31*, doi:10.1029/2004GL020910.
(77) Jakober, C.; Destaillats, H.; Green, P.; Charles, J. Oxygenated organics compounds present in motor vehicle emissions, AAAR Annual Conference 2003.
(78) Novakov, T.; Corrigan, C. E. Cloud condensation nucleus activity of the organic component of biomass smoke particles. *Geophys. Res. Lett.* **1996**, *23*, 2141−2144.
(79) Andreae, M. O.; Merlet, P. Emission of trace gases and aerosols from biomass burning. *Global Biogeochem. Cycle* **2001**, *15*, 955−966.
(80) Mayol-Bracero, O. L.; Guyon, P.; Graham, B.; Roberts, G.; Andreae, M. O.; Decesari, S.; Facchini, M. C.; Fuzzi, S.; Artaxo, P. Water-soluble organic compounds in biomass burning aerosols over Amazonia − 2. Apportionment of the chemical composition and importance of the polyacidic fraction − art. no. 8091. *J. Geophys. Res., [Atmos.]* **2002**, *107*, 8091.
(81) Reid, J. S.; Koppmann, R.; Eck, T. F.; Eleuterio, D. P. A review of biomass burning emissions part II: intensive physical properties of biomass burning particles. *Atmos. Chem. Phys.* **2005**, *5*, 799−825.
(82) Sakurai, H.; Tobias, H. J.; Park, K.; Zarling, D.; Docherty, S.; Kittelson, D. B.; McMurry, P. H.; Ziemann, P. J. On-line measurements of diesel nanoparticle composition and volatility. *Atmos. Environ.* **2003**, *37*, 1199−1210.
(83) Tobias, H. J.; Beving, D. E.; Ziemann, P. J.; Sakurai, H.; Zuk, M.; McMurry, P. H.; Zarling, D.; Waytulonis, R.; Kittelson, D. B. Chemical analysis of diesel engine nanoparticles using a nano-DMA/thermal desorption particle beam mass spectrometer. *Environ. Sci. Technol.* **2001**, *35*, 2233−2243.
(84) Decesari, S.; Facchini, M. C.; Matta, E.; Mircea, M.; Fuzzi, S.; Chughtai, A. R.; Smith, D. M. Water soluble organic compounds formed by oxidation of soot. *Atmos. Environ.* **2002**, *36*, 1827−1832.

Received for review September 14, 2004. Revised manuscript received April 11, 2005. Accepted April 26, 2005.

ES048568L